10/19/95

SANDIA REPORT

SAND94–2283 • UC–814
Unlimited Release
Printed September 1995

Yucca Mountain Site Characterization Project

Preliminary Geostatistical Modeling of Thermal Conductivity for a Cross Section of Yucca Mountain, Nevada

C. A. Rautman

Prepared by
Sandia National Laboratories
Albuquerque, New Mexico 87185 and Livermore, California 94550
for the United States Department of Energy
under Contract DE-AC04-94AL85000

"Prepared by Yucca Mountain Site Characterization Project (YMSCP) participants as part of the Civilian Radioactive Waste Management Program (CRWM). The YMSCP is managed by the Yucca Mountain Project Office of the U.S. Department of Energy, DOE Field Office, Nevada (DOE/NV). YMSCP work is sponsored by the Office of Geologic Repositories (OGR) of the DOE Office of Civilian Radioactive Waste Management (OCRWM)."

Issued by Sandia National Laboratories, operated for the United States Department of Energy by Sandia Corporation.

Available to DOE and DOE contractors from
Office of Scientific and Technical Information
PO Box 62
Oak Ridge, TN 37831

Prices available from (615) 576-8401, FTS 626-8401

Available to the public from
National Technical Information Service
US Department of Commerce
5285 Port Royal Rd
Springfield, VA 22161

NTIS price codes
Printed copy: A04
Microfiche copy: A01

DISCLAIMER

Portions of this document may be illegible in electronic image products. Images are produced from the best available original document.

SAND94-2283
Unlimited Release
Printed September 1995

Distribution
Category UC-814

Preliminary Geostatistical Modeling of Thermal Conductivity for a Cross Section of Yucca Mountain, Nevada

Christopher A. Rautman
Geohydrology Department
Sandia National Laboratories
Albuquerque, New Mexico 87185

Abstract

Two-dimensional, heterogeneous, spatially correlated models of thermal conductivity and bulk density have been created for a representative, east-west cross section of Yucca Mountain, Nevada, using geostatistical simulation. The thermal conductivity models are derived from spatially correlated, surrogate material-property models of porosity, through a multiple linear-regression equation, which expresses thermal conductivity as a function of porosity and initial temperature and saturation. Bulk-density values were obtained through a similar, linear-regression relationship with porosity. The use of a surrogate-property allows the use of spatially much-more-abundant porosity measurements to condition the simulations. Modeling was conducted in stratigraphic coordinates to represent original depositional continuity of material properties and the completed models were transformed to real-world coordinates to capture present-day tectonic tilting and faulting of the material-property units. Spatial correlation lengths required for geostatistical modeling were assumed, but are based on the results of previous transect-sampling and geostatistical-modeling work.

The two-dimensional material-property models appear to be reasonable numerical representations of the layered tuffaceous geology of Yucca Mountain. Visually, the models reflect the character of known geologic units, and statistically, the models as a whole replicate the distribution and statistics of the input porosity data used to condition the simulations. Heterogeneity, both lateral and vertical, is consistent with observed variation in the available drill-hole porosity information. Preliminary sensitivity analyses indicate that the transformation of porosity to thermal conductivity is most sensitive to variations in the in-situ saturations of the welded and nonwelded rock types present at Yucca Mountain.

This work was performed under the guidance of the U.S. Department of Energy, Office of Civilian Radioactive Waste Management, Yucca Mountain Site Characterization Project, under contract DE-AC04-94AL85000. The scientific investigation discussed in this report is covered under the description of work for WBS 1.2.3.2.2.2.2. The planning document that directed this work activity is WA-0015.

Table of Contents

List of Figures

List of Color Plates

List of Tables

Preliminary Geostatistical Modeling of Thermal Conductivity for a Cross Section of Yucca Mountain, Nevada

Introduction

The potential high-level nuclear waste repository at Yucca Mountain, Nevada (fig. 1), will impose a significant thermal load on the enclosing rocks. This heat will create a number of stresses on the natural system, ranging from thermally driven expansion of the rock mass to the possible induction of thermally driven convection cells within the hydrologic system. The ability of the host rocks to dissipate this thermal loading is thus of significant interest to engineering and performance-assessment studies of the Yucca Mountain site.

Simple conduction of heat through the rock matrix is one major mechanism of dissipating the heat deposited in the rocks by hot waste. Heat-conduction codes, such as COYOTE-II (Gartling and Hogan, 1994), require numerical input models of thermal conductivity and other physical properties of the rock mass. Preliminary thermal-conduction modeling is being conducted to assess the effects of various assumptions with respect to the magnitude and spatial distribution of input material properties (Longenbaugh and others, 1995). Typical assumptions being evaluated include (1) the use of a domain characterized by uniform physical properties set equal to some average or "representative" value; and (2) use of a horizontally layered approximation of a heterogeneous geologic system, where the layers are represented by uniform fields of average properties. Closer approximation of actual geologic conditions may be achieved (3) by using dipping, rather than computationally more efficient horizontal, uniform-property layers.

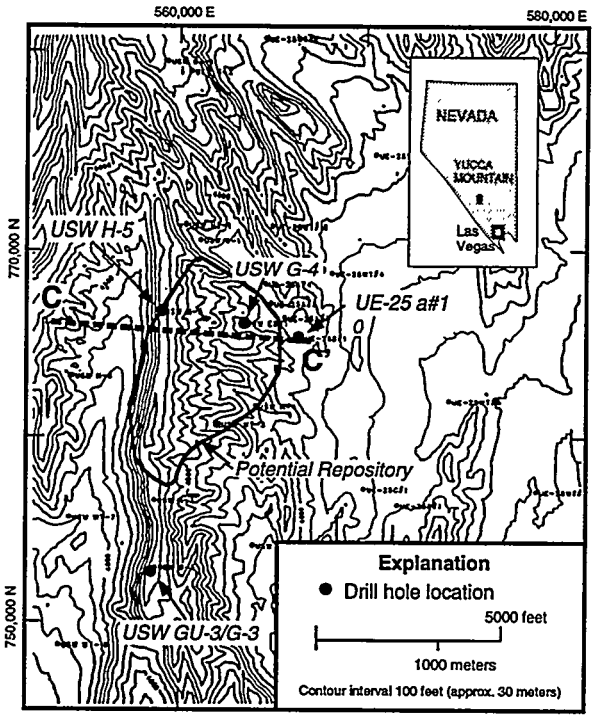

Figure 1. Index map showing the potential Yucca Mountain high-level nuclear-waste repository site in southern Nevada, and the location of the cross section for which thermal-properties modeling was conducted.

Additional complexity may be added through the use of time-varying material properties (actually temperature-varying in response to transient thermal loading).

The three types of spatial models of physical properties discussed in the preceding paragraph are all rather simplified representations of the actual geologic environment at Yucca Mountain. Although the different geometric representations described above unquestionably affect the modeling of heat conduction away from a hot repository,

another, perhaps more significant factor affecting the computational results is the use of averaged, or so-called "representative," material properties. This approach to modeling a spatially heterogeneous domain is widely applied, and it is appropriate in many instances, particularly early in the design of an engineering project. Increasingly, however, it has become apparent that the use of averaged material properties may significantly distort predictions of the actual performance of a natural system with respect to some physical process.

Recognition of this potential distortion has been particularly widespread in hydrology, where it has been noted that in some geologic environments ground-water flow patterns may be essentially unrelated to the "average" permeability. Water flows preferentially through regions of high permeability, and if those conductive zones are spatially correlated, the occurrence of large zones of impermeable material may be completely irrelevant to the flow process. The physical process may be dominated by a small fraction of the extreme tail of the spatial distribution of values. The conceptual process used to develop the supposedly representative material properties, usually simply some form of averaging, generally does not consider these extreme values (which may be either high values or low). Thus, property values must be considered in the context of the specific physical process under investigation in order to be considered "representative." An alternative approach is to model explicitly the complete spatial variability of the domain and to let the physical-process algorithm identify the effect of the extreme values.

Numerical representation of the physical process under investigation may impose constraints on the degree of detail and heterogeneity that can be captured by material-property models. Greater physical heterogeneity typically requires use of finer grid spacings and smaller time steps in computational codes, and limits on computing power may preclude the analysis of highly complex geologic models. As computers continue to increase in speed and availability of memory, these computational constraints become less restrictive, and the evaluation of more geologically realistic models becomes feasible.

To assess both the effect of spatially correlated material properties that incorporate the full range of variability observed in nature and the impact of this increased level of detail on computational resource requirements, we have developed preliminary heterogeneous models of thermal conductivity and other physical properties for a simplified geologic cross section of Yucca Mountain (fig. 2). Several different models are presented and three distinctly different models have been used as input to heat-conduction codes for comparison with the results of more simple calculational models. Together, the different models provide a first-pass sensitivity analysis of heat conduction to different types of spatial heterogeneity (Longenbaugh and others, 1995).

Conceptual Framework for Thermal-Properties Modeling

Although quantitative thermal-property data from Yucca Mountain are rather limited, both in terms of the number and distribution of the available drill holes and vertically within those drill holes, there is a wealth of geologic information available from the site that bears on modeling spatial heterogeneity. It is possible to build upon this site-specific geologic data, as well as upon broader-based geologic knowledge of volcanic systems similar to Yucca Mountain, to develop a conceptual model of spatial heterogeneity that can be modeled quantitatively.

First and foremost, the geology of Yucca Mountain is a layered system (figs. 2

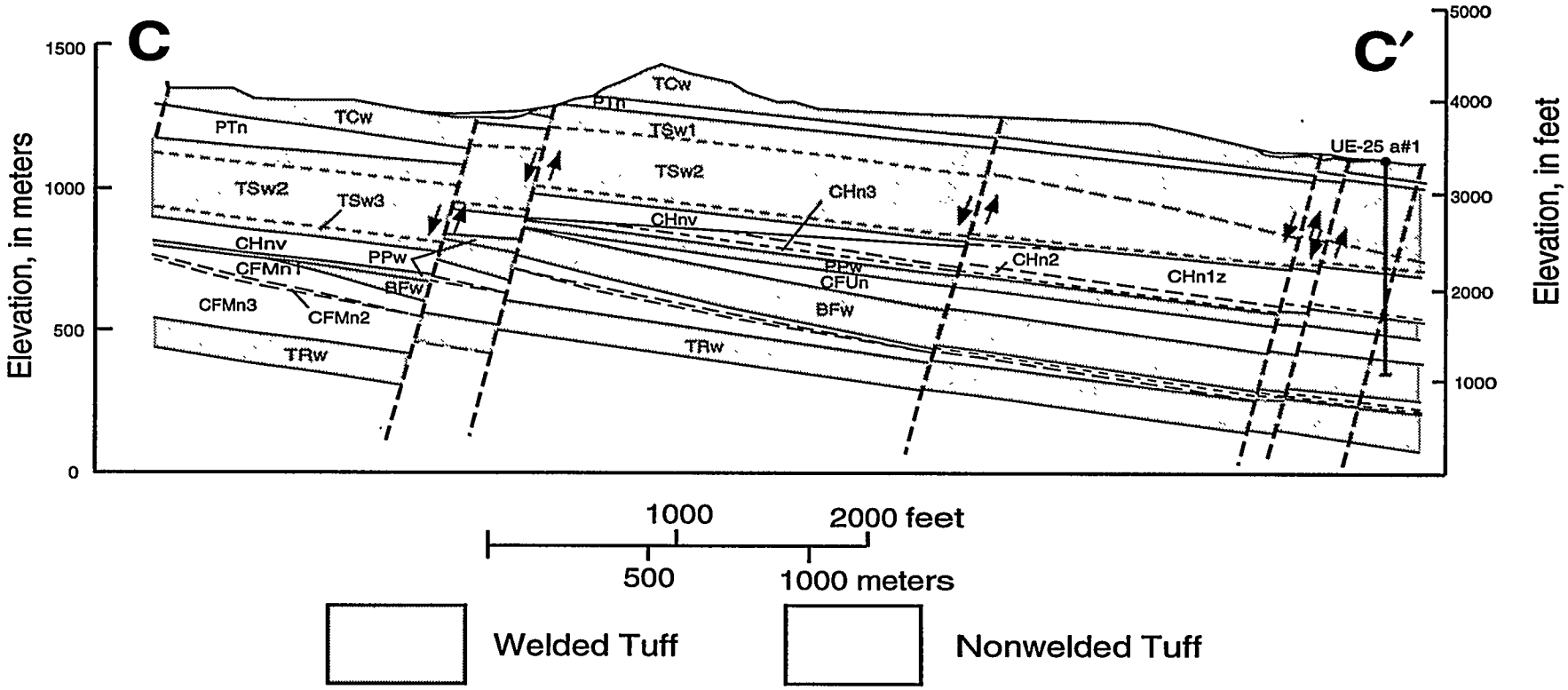

Figure 2. Geologic cross-section of the northern portion of the potential repository region at Yucca Mountain corresponding to section C—C′ of Brandshaug, 1991 (see fig 1, this report). Stratigraphic units are thermal/mechanical units (Ortiz and others, 1985) described in figure 3. Welded intervals are shaded.

and 3). The major ash-flow genetic units that compose the bulk of the rocks present to depths of several thousand meters are the deposits of near-instantaneous volcanic eruptions that produced widespread, sheet-like deposits. Thicknesses of these first-order layers vary from approximately 100 to 300 meters. The large-volume ash-flow deposits are separated from one another by thinner and more lithologically diverse tuffaceous and reworked deposits that vary in thickness from a few meters to several tens of meters. The large-volume ash-flow deposits were emplaced as hot, plastic masses of volcanic shards and other fragments. During cooling from magmatic temperatures, these deposits compacted and welded under their own weight, and underwent various other types of alteration. Because of the sheet-like nature of the ash-flow units, environmental conditions within these deposits during cooling and alteration generally were relatively constant horizontally, and varied most rapidly in a vertical direction. Cooling and alteration phenomena, which collectively influence the thermal properties of specific rock samples through the density and specific resultant mineral assemblages, appear to have produced an internal zonation of the major ash-flow tuff stratigraphic units in which intervals of similar rock characteristics are on the order of a few meters to several tens of meters in thickness (e.g., Scott and Bonk, 1984). Material properties typically appear to be well correlated spatially with some of these zonal units (Rautman and others, 1991). Some of the stratigraphic names that have been applied to the various subdivisions of the lithologic sequence at Yucca Mountain are shown schematically in figure 3.

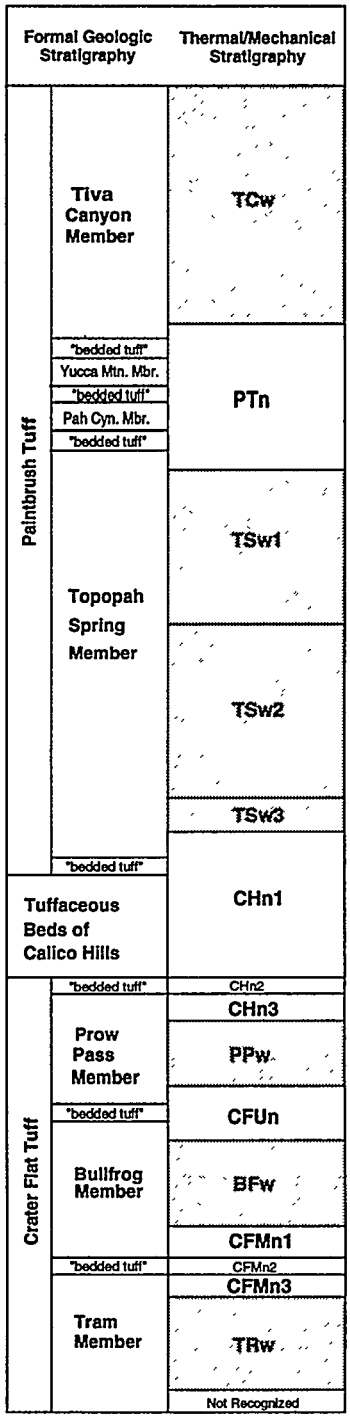

Figure 3. Schematic stratigraphic column for Yucca Mountain and vicinity showing stratigraphic nomenclature in general use. Correlation of units follows original definitions found in table 1 of Ortiz and others (1985). Welded intervals are shaded and correspond to those in figure 2.

Secondly, examination of drill core from Yucca Mountain and evaluation of quantitative material-properties data taken from that core indicates that there is significantly greater vertical heterogeneity than typically has been captured by most "layered" geologic

models, such as Ortiz and others (1985), Wittwer and others (1992), and Buesch and others (1993). This small-scale vertical heterogeneity gives rise to a wider range of values than can be captured by the vertical averaging process generally used to develop "representative" material properties. Because the physical conditions responsible for development of those variable properties unquestionably were extensive laterally, we can assume that observed (sampled) material-property values correlate for some substantial lateral distance away from our limited number of drill-hole sampling locations. Thus even if the sample data are insufficient to develop a rigorously quantitative model of spatial continuity in the horizontal direction, it is likely that the range of spatial correlation is quite large laterally, and that the anisotropy ratio of horizontal-to-vertical correlation lengths is a large value.

Another phenomenon observable in available material properties data from Yucca Mountain is that changes in properties across most unit boundaries typically are somewhat gradational (Rautman and Flint, 1992), rather than abrupt at a knife-edge contact. This gradational nature of material-properties change follows logically as well. If the physical processes affecting the cooling and altering mass of compacting volcanic debris are subregional in extent and are related to the overall ash-flow deposit geometry, it is unlikely that those physical conditions would change abruptly. Thus, with limited exceptions related to erosional surfaces and cooling breaks, transitional contacts between material-property units should be the rule, rather than the exception. Transitional contacts between "units" of similar (but still heterogeneous) properties may have computational benefits, in that the physical process must be numerically modeled over a (relatively) gradually changing set of material properties. Numerical difficulties associated with abrupt changes in input properties may be minimized.

Geostatistical Methods

The conceptual model of a layered tuffaceous system, with laterally extensive spatial correlation of vertically variable material properties, has been used to guide construction of the heterogeneous, spatially correlated material-property models. Geostatistical methods provide a relatively rigorous, quantitative framework for analyzing and modeling spatially distributed data. Spatial correlation is induced in geostatistical models through use of a generalized form of linear, least-squares regression, known as kriging. The required spatial covariance matrix is computed from a descriptive covariance function, generally referred to as the *variogram*, $\gamma(\mathbf{h})$, which is given by

$$2\gamma(\mathbf{h}) = \frac{1}{N}\sum_{i=1}^{N}[Z(\mathbf{x}_i) - Z(\mathbf{x}_i+\mathbf{h})]^2, \quad (1)$$

where $Z(\mathbf{x})$ is the value of the variable of interest observed at spatial location $\mathbf{x}$, and $Z(\mathbf{x}+\mathbf{h})$ is the value observed at some vector distance, $\mathbf{h}$, away from $\mathbf{x}$ (Journel and Huijbregts, 1978). For a spatially correlated variable, differences in value of the variable are typically small at small separations, and these differences tend to increase with increasing separation distance, $\mathbf{h}$. At a distance beyond the range of correlation, the squared differences in value, $[Z(\mathbf{x}) - Z(\mathbf{x}+\mathbf{h})]^2$, are generally observed to stabilize about a near constant value, which is theoretically equal to the univariate variance of the data, σ^2. Note that because $\mathbf{h}$ is a vector quantity, the range of spatial correlation may be different in different directions (i.e., anisotropic).

An important distinction in geostatistics is the difference between estimation and simulation. If the kriging algorithm is applied directly to observed data values, the modeling approach is referred to as *estimation*, and the result at any unsampled spatial location is a value in the units of the variable itself. If the

algorithm is applied to the relative positions of the data on the cumulative-distribution function (cdf) of the variable, the result is the expected position of the unsampled location on the cdf, *conditional to the surrounding observed data*. This position on the cdf can be interpreted as a probability of occurrence, and if the form of the cumulative probability distribution is known (or can be assumed), an actual value of the variable of interest to represent that unsampled location may be obtained by sampling from the cdf, given the conditional probability. This modeling approach is termed *conditional simulation*. Theoretically, the value obtained by direct estimation of the original variable can be shown to be the conditional expectation of the cdf representing the distribution of all possible values for that variable (Deutsch and Journel, 1992), and across a large number of different simulations, the average simulated value can be observed to converge on the estimated value.

Because spatial correlation of extreme values of thermal conductivity may exert a dominating influence on the (numerically modeled) thermal conduction process, geostatistical simulation was selected as the preferred technique for modeling material properties for input to the thermal-modeling codes. This is the case even though the usual focus of a geostatistical simulation exercise, i.e., the assessment of geologic uncertainty resulting from "incomplete" physical sampling, was not a primary emphasis of this modeling work. Whereas estimation always results in what is effectively an "expected" or average value, simulation is not so constrained. Once the conditional probability-density function of the unsampled location is identified, the actual value modeled at that location is generated by sampling randomly from the probability distribution. Although extreme values (high or low) may be relatively rare, there is a finite probability that such a value may exist at any unsampled location. Once any value has been simulated, that value will propagate through the simulated field as dictated by both the spatial correlation pattern and the other values used to condition the field. One standard test of a simulated field is to compare the resulting histogram with the histogram of the conditioning data to ensure that this known attribute of the actual data is being reproduced.

Construction of Geostatistical Models

Construction of the geostatistical models had to be matched to the specific input requirements of the thermal heat-conduction code (COYOTE-II; Gartling and Hogan, 1994) that was used to evaluate the resulting material-property models. Specifically, COYOTE-II requires input models of thermal conductivity and heat capacity for every point within the model domain. These material-property models must be mapped onto an appropriate finite-element mesh, which in itself imposes requirements on the format of those material-property models (Longenbaugh and others, 1995, Appendix B). Construction of the geostatistical models is also strongly influenced by the material-property data available for their construction. In this section, we discuss the model domain chosen for the thermal analyses and the use of a stratigraphic coordinate system. We also discuss the available thermal conductivity data and the requirement that conductivity be modeled using a surrogate physical property, in this case, porosity. Also described is the geostatistical simulation process itself; the spatial-correlation model used in that simulation process, the discrimination of differing rock types, based on porosity, for conversion to thermal conductivity values; and the coordinate conversions necessary to impose post-depositional structure on the models.

Model Domain

The physical domain of the geostatistical model was selected to correspond as closely as possible to a cross section previously modeled using homogeneous material properties and layered uniform properties (Brandshaug, 1991). The new model domain is based on an east-west cross section of Yucca Mountain (fig. 2), originally described as cross section C—C′ of Brandshaug. This model domain, which has been extended beyond the original cross section to include the thermal far field, is described by a local coordinate system with an origin at Nevada State Plane Coordinates (defined in feet) of approximately 766,250 N, 553,150 E. The region of principal interest extends generally eastward from an x-coordinate on this cross section of 1,000.0 m to 4,150.0 m. A two-dimensional grid was defined on this cross section consisting of 100 nodes in the horizontal dimension and 150 modes vertically. Node spacings are 31.5 m horizontally and 11.0 m vertically. These spacings were selected to correspond approximately to the smallest-resolution finite-element mesh previously used in the layered, homogeneous-property thermal model. The intent was to allow the geostatistical grid to be mapped directly onto the finite-element mesh (Longenbaugh and others, 1995, Appendix B) in the near-field region of steepest induced thermal gradients, and to allow averaging of material properties onto a coarser grid outward into the far field where thermal gradients are significantly smaller. Regions surrounding the geostatistical model at large distances were assigned constant material properties representative of welded tuff.

Because the tuffs at Yucca Mountain have been offset by Basin-and-Range faulting and now form a series of east-dipping fault blocks, it was decided to generate the material-property model in "stratigraphic coordinates," representing original depositional continuity, and to impose the tectonic tilting and offset in a deterministic manner on the resulting spatial field. A simplified form of stratigraphic coordinates was chosen, which consisted simply of measuring all vertical distances relative to a well-defined stratigraphic horizon, the base of the welded unit of the Tiva Canyon Member (TCw). Therefore, elevations (z-coordinates) are positive within the Tiva Canyon welded interval and negative in all underlying units. X-coordinates were maintained as the distance along the two-dimensional cross section. Data limitations indicated that a more sophisticated adaptation of the stratigraphic coordinate system, one in which a basal horizon is selected as well and the z-coordinates normalized to between zero and one in order to eliminate the effects of regional thickness variations, was not warranted. Whereas the base of Tiva Canyon welded horizon is encountered in virtually all drill holes at Yucca Mountain, a similar deeper horizon could not be identified because the available drill holes vary markedly in total depth (note: also see discussion of hole GU-3/G-3 on page 15).

The stratigraphic grid is illustrated schematically in figure 4. To correspond with the indexing conventions of the geostatistical simulation algorithms, the origin of the geostatistical grid is at (1,000,–1485) m.

Material-Property Data

Thermal conductivity is a material property that determines the amount of heat that will flow through an object when a temperature difference exists across the object. It is, perhaps, the most important material property in modeling thermal conduction. Actual laboratory measurements of thermal conductivity are quite limited at Yucca Mountain. Many of the thermal conductivity data that have been obtained thus far are from drill holes which are not located on the cross section of interest. Fortunately the available data indicate

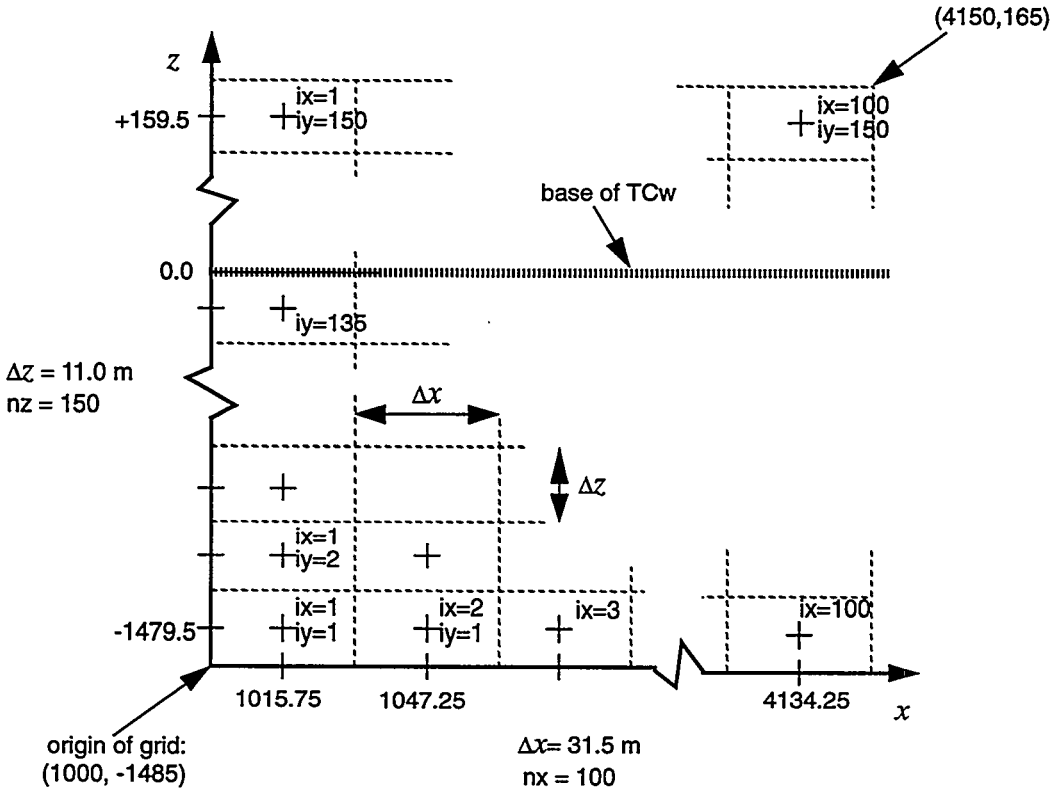

Figure 4. Schematic representation of geostatistical grid and stratigraphic coordinates used for geostatistical modeling of thermal properties cross section. Elevations (*z*-coordinate) are measured relative to the base of Tiva Canyon welded (TCw) thermal/mechanical unit (heavy dotted line). Simulated points (+) are indexed according to the (ix, iy) scheme within the geostatistical algorithms. All dimensions and coordinates in meters. Not to scale.

that thermal conductivity is at least partially correlated with porosity, a framework material property for which data are widely available at the site. It is thus possible to create detailed surrogate models of porosity, which can then be converted to values of the desired property, thermal conductivity.

Porosity Surrogate for Thermal Conductivity

Thermal conductivity values have been measured on a number of samples from a single drill hole, USW NRG-6 (C.S. Chocas, SNL, written communication, 1994), which is located some 450 m north of the modeled cross section. Thermal conductivity was measured at several different steady-state temperatures, both below (30°C, 50°C, and 70°C) and above (110°C, 155°C, 200°C, 245°C, and 290°C) nominal boiling conditions. Samples were measured under fully saturated, oven-dried, and intermediate (air dry) conditions, using the guarded heat-flow meter method (ASTM, 1977, as modified for rock specimens). Porosity and bulk density of the tested samples were determined as part of the saturation process.

Multiple linear regression analyses of thermal conductivity values against porosity and the various initial test conditions indicate that the relationship is of the form:

$$k_t = C_0 + C_1 T + C_2 S + C_3 \phi, \qquad (2)$$

where ϕ is porosity, S is saturation, and T is temperature. A different functional relationship is observed for welded and nonwelded tuffs. The coefficients, C_0, C_1, C_2, and C_3, determined for equation (2) are given in table 1.

The degree of correlation requires some comment, given the somewhat disparate multiple r^2 values observed for welded versus nonwelded tuffs. Both r^2 values need to be taken somewhat cautiously. The regressions for samples of nonwelded tuff are based upon a very small number of actual core samples. Because thermal conductivity is a function of several parameters, each physical core specimen has been tested under multiple test conditions. Thus, the actual range of porosity values examined at this time is somewhat limited, even though that range of porosities is believed to be typical of the range of values existing at Yucca Mountain. There are also other difficulties with the regressions, particularly with respect to non-normality of the residuals from the regressions. Despite the limitations of the actual data and concerns regarding the statistical analyses, simple visual plots of the available thermal conductivity data indicate a clear dependency on porosity and saturation. Thus, the coefficients indicated in table 1 are believed to represent a reasonable transformation of porosity to thermal conductivity for a study, whose principal purpose is to examine the *effects* of spatial heterogeneity on temperature distributions, and to compare those effects to models created using other, highly simplified assumptions (note: see additional discussion of this relationship in the Appendix).

The dependency of thermal conductivity on saturation and temperature introduces a need to identify the appropriate physical conditions for the transformation. We have adopted the approach of assuming that it is the initial temperature and saturation which are most significant, and the appropriate thermal conductivity value for each grid node is computed at those initial conditions. Distortions induced in the thermal modeling as a result of changes from this initial state can be assessed through sensitivity studies.

Several different initial temperatures were selected for investigation: 50°C (below onset of boiling of pore water), 100°C (near/at boiling), and 110°C (no pore water remaining). Ultimately, however, thermal modeling (Longenbaugh and others, 1995) focused solely on the 50°C thermal-conductivity-conversion models, as this is an approximation of the in-situ temperature prior to construction of a repository. This temperature was also the

Table 1: Coefficients of Multiple Linear Regressions Relating Thermal Conductivity and Porosity (C.S. Chocas, SNL, written comm., 1994)

[No. Samples - Number of discrete sample locations taken from the core; No. Analyses - Number of thermal conductivity determinations entered into the regression]

Coefficient	Low Temperature, $T \leq 100$ °C		High Temperature, $T > 100$ °C	
	Welded	Nonwelded	Welded	Nonwelded
C_0	1.748	1.250	1.916	1.039
C_1	3.529×10^{-4}	2.096×10^{-3}	-1.564×10^{-4}	3.370×10^{-4}
C_2	0.4347	0.5853	0	0
C_3	-3.210	-2.238	-4.055	-1.530
No. Samples	38	7	20	3
No. Analyses	78	204	135	29
Multiple r^2	0.58	0.95	0.47	0.99

median, non-boiling temperature used in laboratory testing (C.S. Chocas, SNL, written communication, 1994).

The issue of initial saturation is considerably more complicated, in that saturation is a function of intrinsic rock properties (specifically of porosity) and the location-specific operation of the hydrologic system. For a rock with a specified amount of pore space, the actual saturation will vary with proximity to the static water table and with local infiltration conditions. For this reason, saturations were arbitrarily set to 60 percent for purposes of converting porosity to thermal conductivity. This value is somewhat generalized saturation for both welded and nonwelded materials in drill hole USW UZ-16 (fig. 5). However, as suggested by the available saturation data, saturations may be quite different in welded and nonwelded rocks. As a sensitivity study, porosity data were converted to thermal conductivity values at more reasonable differential saturations of 80 percent in welded units and 40 percent in nonwelded intervals. However, initial thermal modeling (Longenbaugh and others, 1995) was restricted to the equal 60-percent saturation property models.

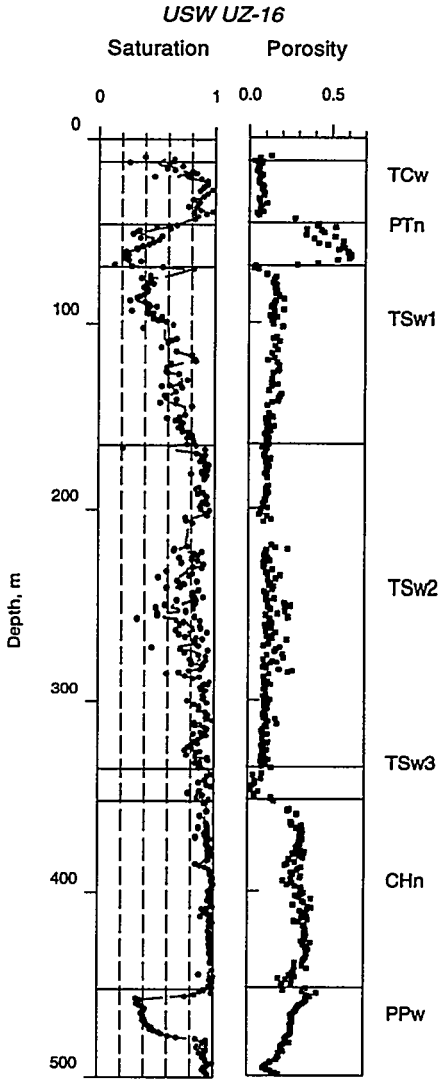

Figure 5. Saturation and porosity profiles for samples from drill hole USW UZ-16 (L. E. Flint, USGS, written communication, 1994). Saturation is a complex function of position relative to the water table and of stratigraphic unit and porosity.

Porosity-Bulk Density Relationship

Porosity is particularly strongly correlated with bulk density across a wide range of degrees of welding, and thus, of porosity (Rautman and others, 1995). This relationship is of the form:

$$\rho_b = 2.35 - 2.40\phi \ , \qquad (3)$$

where ρ_b is bulk density and ϕ is porosity. This regression relationship has a coefficient of determination (r^2) of 0.993. Bulk density can be related to heat capacity (ρc_p), which is another of the physical properties required in the heat-conduction codes, simply by multiplying ρ_b by the specific heat (c_p) of the rock,

$$\rho c_p = \rho_b c_p \ . \qquad (4)$$

Porosity Information

Measurements of porosity were compiled from seven drill holes of in the general vicinity of the desired cross section (Schenker and others, 1995, based on information from: Anderson, 1981, 1984; L. E. Flint, USGS, written comm., 1994; Flint and Flint, 1990;

Knauss and Peifer, 1986; Knauss and others, 1985; Lin and Daily, 1984; Peters and others, 1984; Rush and others, 1983; Schwartz, 1990; Weeks and Wilson, 1984; Yucca Mountain Project, 1992). A number of problems were encountered in evaluation of the porosity data. Specifically, the data reported represent a number of original analyses performed using a variety of different measurement techniques. Additionally, there are duplicate values reported for certain drill-hole intervals; it is unclear if these multiple values reported for a given depth in a drill hole represent replicate measurements on the same, identical specimen, or if the data represent different subsamples.

To reduce the effects of multiple reported values at the same spatial location, the porosity data were cleaned using the following conventions. First, because they represented a distinct minority of the overall data, duplicates for which the measurement technique was indicated in Schenker and others (1995) as "gas pyncnometry" or "mercury porosimetry" were eliminated in favor of data measured by other techniques (generally identifiable as using some variant of Archimedes' principle). Second, remaining duplicate values at the same depth generally were averaged, assigning equal weights to each. If one of several values was clearly different from two or more other data (and from other nearby measurements), it generally was eliminated prior to averaging. These edited data formed the basis for further evaluation, and they are displayed graphically in figure 6.

Because the porosity data are used to condition geostatistical models in a effort to create a numerical representation of a conceptual model of Yucca Mountain consisting of alternating layers of welded and nonwelded tuff, the graphical display of figure 6 was examined for evidence of this conceptual model. Generally, there is convincing evidence that the porosity data are capturing the conceptual geologic model. The cored drill holes (all except USW H-1), for which there are reasonably adequate data, strongly support the earlier subdivision of the stratigraphic interval by Ortiz and others (1985) into alternating high-porosity nonwelded and low-porosity welded increments.

Geostatistical simulation relies upon the conditioning data to impart the appropriate values and statistical character to the resulting numerical models of material properties. A statistical summary of the porosity data is presented in table 2 (first column), and the univariate histogram of the values is presented in figure 7. The histogram is notable in that the bimodal nature of the data is particularly apparent. The mode corresponding to a porosity of 10–12 percent represents the welded tuffs in the section, whereas the broad mode centered at about 30 percent porosity corresponds to the nonwelded intervals that separate the major ash-flow sequences. The welded mode dominates the univariate distribution (a) because the overall stratigraphic section is dominated volumetrically by this rock type

Table 2: Selected Statistical Measures for Porosity Data

[Porosity data as a fraction; Std.Dev. - standard deviation; C.V.- coefficient of variation, a standardized measure of variability, is defined as the standard deviation divided by the mean; N - number of samples]

	All Available Porosity Data	Porosity Data for Single Composite Drill Hole	Porosity Data for Drill Holes G-3, G-4 and a#1
Mean	0.216	0.186	0.203
Std. Dev.	0.106	0.107	0.116
C.V.	52.4%	57.3%	57.0%
Maximum	0.650	0.650	0.650
Median	0.177	0.160	0.166
Minimum	0.014	0.018	0.014
N	1015	513	586

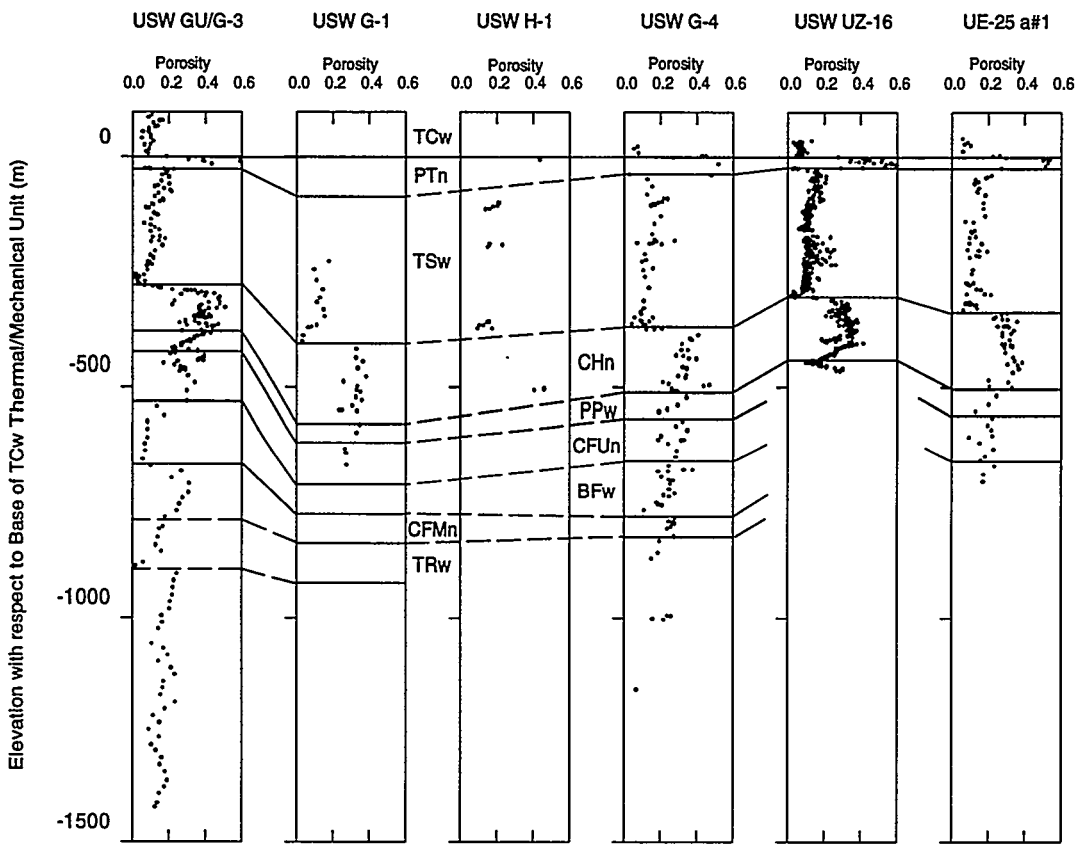

Figure 6. Porosity data for selected drill holes at Yucca Mountain. Drill-hole plots are arranged in correct horizontal sequence from west (left) to east (right) to correspond to modeled cross section (horizontal separations not to scale). Depths are measured in stratigraphic coordinates (see text) corresponding to distance above (below) the base (heavy horizontal line) of Tiva Canyon welded thermal/mechanical unit (TCw).

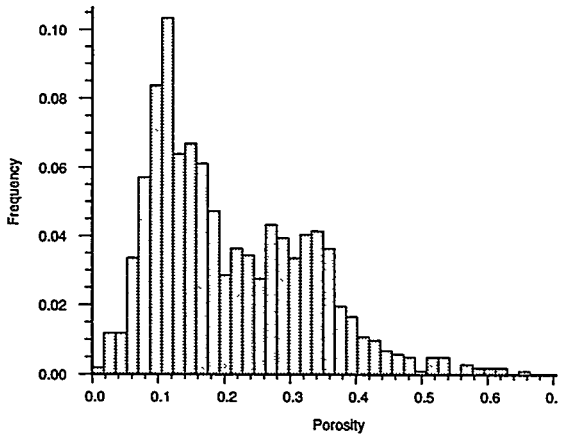

Figure 7. Histogram of all available porosity data (compiled by Schenker and others, 1995).

and (b) because the sampling pattern is not completely unbiased. Some of this bias arises from the fact that the Topopah Spring welded thermal/mechanical unit (TSw) has been the focus of increased sampling because of its designation as the potential repository horizon. Additional bias probably arises from the markedly different down-hole sampling densities in the various holes (fig. 6). In particular, the significantly denser sampling of the TSw unit in drill hole USW UZ-16, in conjunction with the lack of such sampling in the lower nonwelded units underlying the CHn thermal/mechanical unit, appears to have biased the histogram of figure 7.

To reduce the effects of sampling bias on the resulting models and in keeping with the objectives of this preliminary modeling effort—the evaluation of the influence of heterogeneous material properties on thermal profiles—two different sets of conditioning data were generated from the porosity information. First, a single, composite drill hole was created to condition a "perfectly" layered, but heterogeneous, material-properties model. The purpose of this composite drill hole was to capture the best *conceptually* possible numerical representation of the entire stratigraphic interval. A second set of conditioning data was generated to provide a more geologically realistic representation of Yucca Mountain. In this latter scenario, additional spatial heterogeneity departing from the perfectly layered case is allowed.

Single Composite Drill Hole

The modeled cross section passes very near drill holes USW H-5 (on the west), USW G-4, and UE-25 a#1 (fig. 1). Of these drill holes, USW G-4 has the most complete set of porosity measurements. Therefore, data from G-4 formed the principal basis of the composite drill hole. Examination of porosity data from drill hole G-4 in figure 6 indicates that the conceptual, interlayered model of Yucca Mountain is somewhat difficult to distinguish at deeper stratigraphic levels. Specifically, differences in welding between the Prow Pass and Bullfrog welded thermal/mechanical units and the adjacent nonwelded intervals of the upper and middle Crater Flat Tuff are not well developed. The cause of this apparent failure of the conceptual model for data from drill hole USW G-4 is unclear; however, it is possible that this failure is an artifact related to the fact that data from five separate reports have been combined to represent drill hole G-4. In any event, because the intent of this modeling exercise was to test the implications of a "perfectly-layered" conceptual stratigraphic model, porosity values below –500 m (stratigraphic coordinates) in G-4 were replaced arbitrarily by values taken from the equivalent depth interval in drill hole USW GU-3/G-3[†] (fig. 8(a); compare the two porosity profiles in fig. 6). Porosity data reported for this deep portion of drill hole GU-3/G-3 are taken from a single reference (Anderson, 1984, *in* Schenker, 1995). Any north-to-south trend, or drift, in porosity values involved in this projection of data from drill hole GU-3/G-3 was neglected in light of the magnitude of vertical changes in porosity and the current modeling objectives.

A second complication involving the USW G-4 data results from the logistical artifact that most of the drill holes at Yucca Mountain, including G-4, are located in the bottoms of drainages. Thus they do not penetrate the entire interval of the Tiva Canyon Member tuffs (TCw thermal/mechanical unit). To provide conditioning information with which to model the entire Tiva Canyon interval, an expedient was adopted, whereby porosity data from USW GU-3 were added to the G-4 data for (stratigraphic) elevations above +25 m (fig. 8(a)).

For use as conditioning data, the single-composite drill hole porosity profile was replicated three times along the cross section: at the projected locations of drill holes USW GU-3/G-3, USW G-4, and UE-25 a#1. The spatial position of the conditioning composite-drill-hole information thus corresponds almost identically to the positions of actual drill holes H-5, G-4, and a#1, had these data been available and suitable for use. Because of concern

[†] "Drill hole GU-3/G-3" is actually two separate drill holes located on the same drill pad. Because of logistical problems during drilling, the stratigraphic interval below the water table was cored separately (hole G-3) from the unsaturated-zone portion (GU-3). No core was taken in the upper portion of hole G-3. Because of their close geographic proximity, these holes are generally aggregated and referred to collectively as "GU-3/G-3."

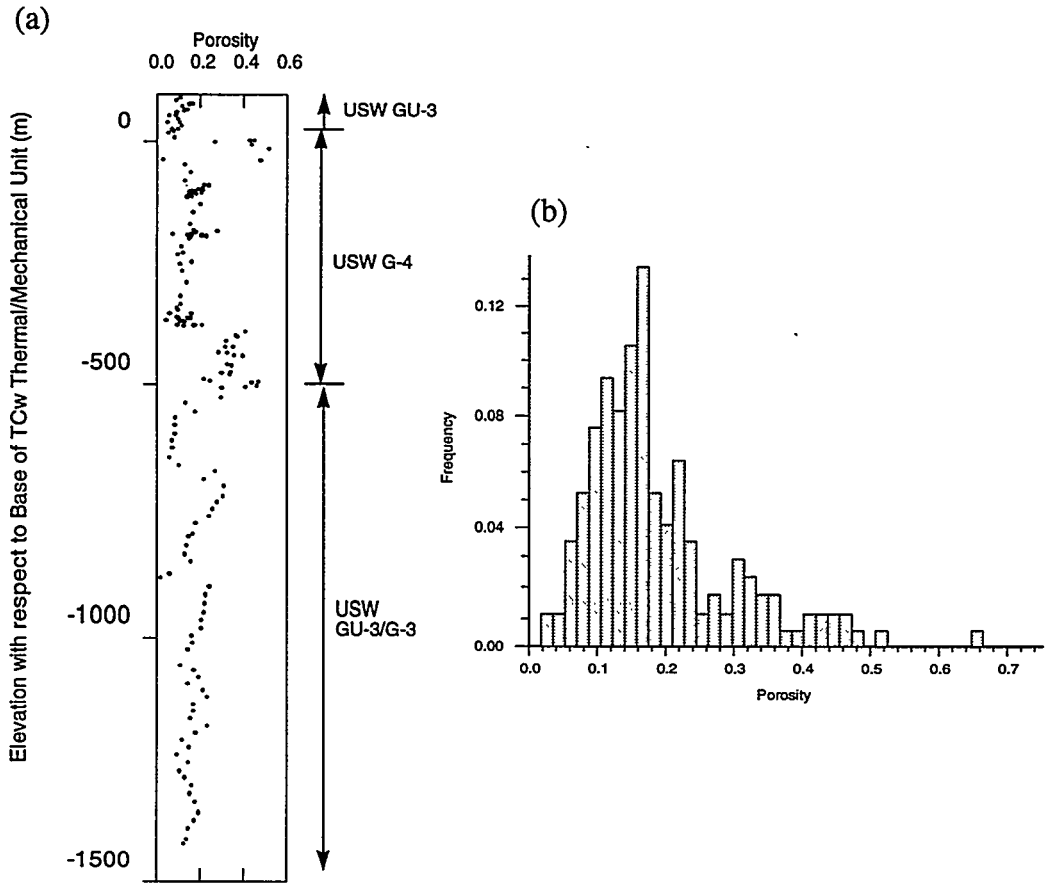

Figure 8. (a) Down-hole plot of porosity values for the composite drill hole set of conditioning data based on segments taken from drill holes USW G-4 and USW GU-3/G-3. (b) Histogram of single drill hole composite porosity data, which include 19 data from hole USW H-1 (see text).

that the exactly replicated composite data might produce numerical artifacts, 19 porosity data obtained from drill hole USW H-1 (fig. 6) were projected onto the cross section in three arbitrary locations between the composite profiles to prevent singularities arising from searches finding only identical conditioning data at the same stratigraphic levels. In retrospect, this precaution appears to have been unnecessary. The statistical summary of the complete set of composite-drill hole conditioning data is given in table 2 (middle column), and the histogram of the porosity values is presented in figure 8(b).

Three-Drill-Hole Composite

The second set of conditioning data used to model porosity for the thermal-properties cross section attempted to use the actual porosity values from drill holes USW GU-3/G-3, USW G-4, and UE-25 a#1, each located at its appropriate, projected spatial position on the cross section. As with the single composite-drill hole case, limitations in the actual data required some manipulation to produce a reasonable set of porosity values for input to the simulation algorithm. As indicated in figure 6, data from the deeper stratigraphic levels of both USW G-4 and UE-25 a#1 are incomplete

or incompatible, strictly speaking, with the layered conceptual model considered applicable to Yucca Mountain. The deep porosity data from drill hole GU-3/G-3 were thus substituted below 500 m (stratigraphic coordinates) in both G-4 and a#1, as was done for the single drill hole composite data. This substitution is of limited significance because this region is within the far field for the thermal calculations. The problem with the eroded upper portion of the Tiva Canyon welded unit similarly was resolved by adding porosity values from the upper part of hole USW GU-3 as before.

A more significant problem involved the projection of data from drill hole USW GU-3/G-3 onto the model cross section. Hole GU-3/G-3 is located some 4.4 km (2.75 miles) to the south of the desired profile. Although the ash-flow tuffs present at Yucca Mountain form regionally extensive sheet-like deposits, a difference in location of this magnitude results in non-trivial thinning, because the direction of transport of the ash flow in this area was to the south, parallel to the direction of projection. Ash-flow tuffs generally thin away from their source caldera. Simple, direct projection of the GU-3/G-3 porosity data onto the model section, as suggested by the drill-hole profile of figure 6, results in major underestimation of the thickness of Topopah Spring tuff present in the western part of the modeled cross section. Accordingly, the thickness of this unit only was scaled to the thickness of the Topopah Spring welded thermal/mechanical unit actually present in drill hole USW H-5, which projects onto the cross section in nearly the same east-west location. Drill hole H-5 is located only 275 m north of the model cross section. Although no core samples or porosity measurements are available from this latter, hammer-drilled hydrologic hole, the cuttings log (Robison and Craig, 1991) does allow interpretation of major lithologic-unit thicknesses. The resulting expansion of the TSw thermal/mechanical unit by some 76 m is portrayed schematically by the arrows in figure 9. The uncorrected porosity plot from GU-3/G-3 is shown on the left-hand side of the figure. The final, adjusted porosity plot for the H-5-corrected pseudo drill hole is shown immediately to the right (second column from left in fig. 9). Also shown on the diagram are the composite porosity data for composite drill holes G-4 and a#1.

The three-drill-hole composite set of conditioning data consists of the porosity information from the three plots on the right-hand side of figure 9. The "extra" porosity values from USW H-1 are *not* included in this set of conditioning data. The statistical summary of the three-drill-hole conditioning data is presented for comparison, also in table 2 (right-hand column). A histogram of the three-drill-hole composite porosity data is presented in figure 10.

Spatial Correlation Model

In a traditional geostatistical modeling exercise, the necessary model of spatial continuity is developed from the available data through a process of modeling sample variograms (equation (1)) computed from the sample data for the variable of interest. This approach was not possible in the current modeling study for two reasons. First, there are insufficient thermal conductivity data to compute reasonable sample variograms. This fact necessitated the use of a surrogate material property, porosity, as the basis of the material-property models. Second, the spatial distribution of porosity data from widely spaced and spatially biased drill holes at Yucca Mountain is insufficient to allow the development of reasonable sample variograms *in the horizontal dimension.* As a consequence of these data limitations, a model of spatial continuity was assumed and used in spatial modeling of material properties for this study.

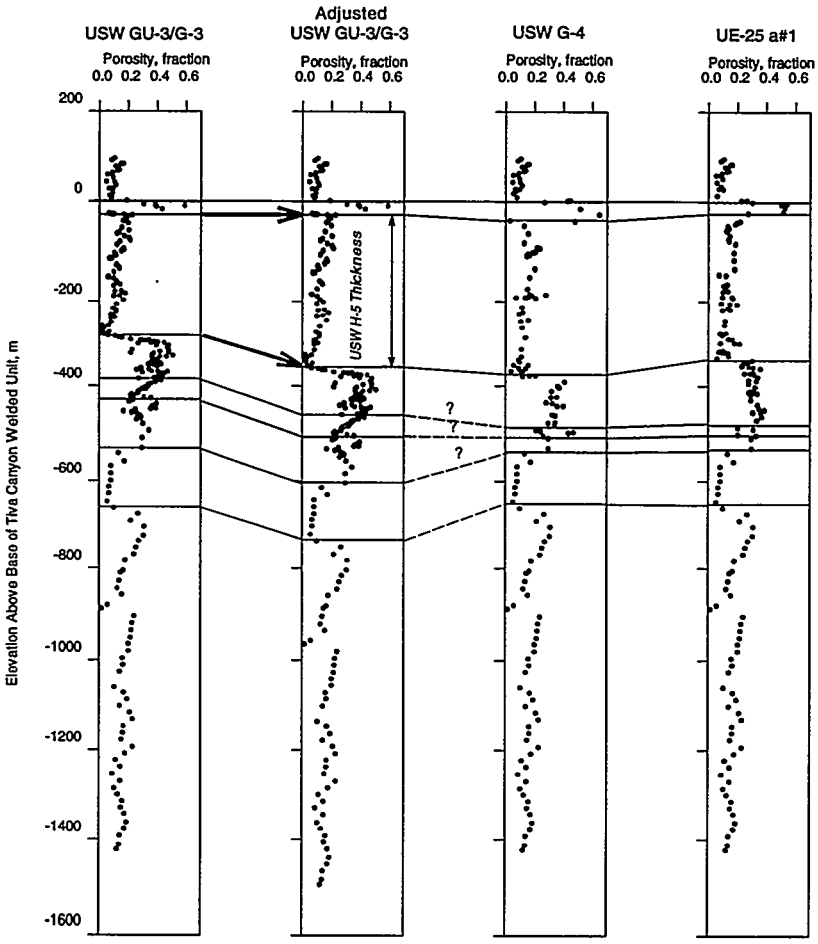

Figure 9. Schematic drill hole cross section showing the three-drill-hole conditioning porosity data. Also shown is the adjustment to the thickness of drill hole USW GU-3/G-3 required by the 4.4 km (2.75 mile) northward projection. Arrows conceptually suggest proportional expansion of the TSw interval actually observed in GU-3/G3 to match that observed in rotary-drill hole USW H-5 (see text).

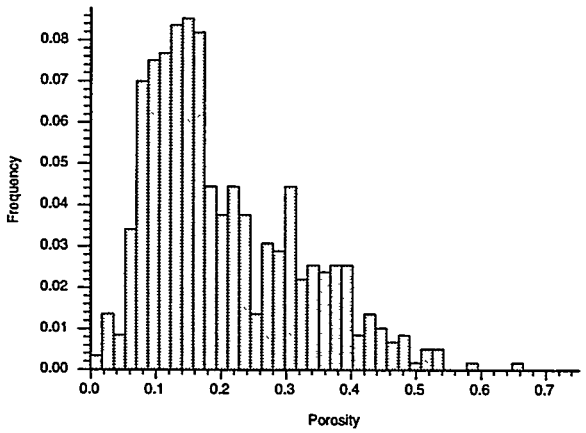

Figure 10. Histogram of the three-drill-hole composite porosity data, based on segments from drill holes USW GU-3/G-3, USW G-4, and UE-25 a#1.

Although the spatial continuity model(s) used to simulate thermal properties are assumed rather than developed explicitly from sample data, they are not without justification. Rautman (1991) reported a range of some 900 m for horizontal correlation of porosity data in one particular unit (CHn1; fig. 3) in an outcrop located northwest of the main Yucca Mountain repository block. Rautman and Flint (1992) summarized the ranges of spatial correlation for porosity observed for a number of mostly vertical outcrop transects at Yucca Mountain. Istok and others (1994) intensively sampled a limited stratigraphic interval and evaluated the lateral continuity of porosity and other hydro-

logic properties both geostatistically and in a deterministic manner. Rautman and Robey (1994) evaluated the spatial correlation of welded and nonwelded rock types as portrayed on published, interpretive geologic cross sections of Yucca Mountain (Scott and Bonk, 1984). Collectively, the pattern which emerges is that porosity is spatially correlated for large (stratigraphically) horizontal distances in the layered volcanic sequence that underlies Yucca Mountain.

Two observations are believed particularly significant. First, Rautman and Robey (1994) reported that welded lithologies appear to be correlated over distances of at least 1,000 m and up to approximately 15,000 m (a two-structure, nested variogram model). That the actual range of correlation is greater than the 1,000-m distance is suggested by their resulting lithologic models, which exhibited more discontinuous lithologic units than expected from field observations. Second, Istok and others (1994) found that porosity data, within the limited stratigraphic interval that they examined, exhibited a *virtually infinite* range of spatial correlation. They observed a prominent vertical trend within their porosity information, which they were able to model successfully with a predictive equation based on relative stratigraphic position. After removing this deterministic component, the residual values from the prediction exhibited relatively small variation about zero and *no spatial correlation* whatsoever. The implication is that almost all horizontal variation could be predicted simply by knowing the vertical position of the sample within the vertical sequence.

For these reasons, and because the resulting models of porosity and thermal conductivity were visually appealing in terms of the conceptual geologic framework of Yucca Mountain, a horizontal range of correlation equal to 5,000 m was adopted for primary modeling purposes by this study. As a sensitivity study, this range was arbitrarily reduced by one-fifth, to 1,000 m, for one model. Vertical variograms were not computed for the composite pseudo-drill-hole data. However, the vertical range of correlation implied by the assumed horizontal correlation lengths was manipulated through use of the horizontal:vertical anisotropy ratio (set at 20:1) to values between that reported for a composite (welded and nonwelded) transect of the Paintbrush Tuff (30 m) by Rautman and Flint (1992) and the thickness of the welded Topopah Spring Member tuffs (300+ m). More sophisticated modeling based upon defensible estimates of actual spatial correlation in the (stratigraphically) horizontal dimensions must await acquisition of additional site characterization information.

Geostatistical Simulation

The conditioning data were "expanded" (Journel and Alabert, 1989) away from their physical position relative to the modeled cross section using the sequential Gaussian simulation algorithm SGSIM, which is part of the GSLIB geostatistical software library (Deutsch and Journel, 1992). Gaussian simulation algorithms make use of the well-known properties of the multivariate Gaussian distribution, which specifies both the relative univariate distribution of values and the degree of spatial correlation exhibited by values of various magnitudes. Gaussian-related algorithms require only an expected value and a variance to fully characterize the univariate histogram, and a single covariance, or variogram, model to fully define the spatial-correlation characteristics of the data (Deutsch and Journel, 1992).

The sequential simulation approach, as implemented in SGSIM, involves discretizing the model domain into a rectangular grid (two-dimensional in the current case) and then defining a random path through that grid, which will visit every grid node once and only

once. At each unsampled node, a simulated value is generated by sampling randomly from the estimated conditional cumulative probability density function (ccdf), which has been conditioned to any nearby data and previously simulated grid nodes found through a specified search process. Functionally, this amounts to kriging the surrounding normal-score-transformed (μ=0, σ^2=1) conditioning values using the correlation structure specified as input, and taking the resulting value as the conditional expectation of a Gaussian distribution (the ccdf). A random number between zero and one is then generated, and the normal-score value corresponding to that position on the ccdf is taken as the simulated value. This location-specific material-property value is added to the grid, and it may serve as part of the conditioning data set for as-yet unsimulated grid nodes. The simulation process then moves to the next location along the random path and the process is repeated. Because simulated values are added to the conditioning data set sequentially, they influence the future simulation of nearby, vacant grid nodes in proportion to the strength of the spatial correlation structure defined for the problem. A spatially correlated field results. At the end of the simulation process, the complete field of normal-score values is back-transformed into the space of the original variable (in this case, porosity).

For the geostatistical models constructed in this study, *at least one observed porosity value* was used in the simulation of each grid node, with a maximum of eight original data. The specified search pattern formed an ellipse 2,000 m by 200 m in radius; the major axis of the search ellipse was stratigraphically horizontal. Up to four previously simulated grid nodes within the search pattern could influence calculation of the ccdf. The requirement that at least one "real" datum enter the probability calculation was imposed to minimize previously observed artifacts that originate from poorly constrained estimates of the ccdf (Rautman and Robey, 1994). If no data are found by the search routine and this requirement is not imposed, a value is generated randomly from the *overall* univariate distribution of values. Such simulated values then enter the set of available conditioning data, and they propagate according to the defined spatial correlation pattern. Although this process is completely consistent with a statistical model of reality, it may lead to the simulation of stochastic rock "units" which are inconsistent with the corresponding conceptual model.

Discrimination of Welded from Nonwelded Rock Type

The transformation of the simulated porosity models to corresponding values of thermal conductivity via equation (2) requires that welded rocks be distinguished from nonwelded materials. This discrimination was accomplished is a straight-forward, if somewhat interpretive, manner for the purposes of this preliminary modeling study, based on the simulated value of porosity. Although arbitrary, the threshold porosity value selected seems remarkably consistent, when viewed in light of the available sample data.

Figure 7 is a histogram of all available porosity data. The distribution of porosity values is distinctly bimodal, with one mode at approximately 10–12 percent representing welded tuffs and a broader mode between roughly 25 and 35 percent representing the more lithologically diverse nonwelded materials. The inter-modal low is somewhat broad and ill defined, but overall there is a clear frequency minimum between 20 and 26 percent porosity. Figure 8 is a histogram representing the distribution of porosity values for the single composite drill hole conditioning data set; this distribution is also distinctly bimodal, capturing the welded/nonwelded nature of the composite lithologic interval. The inter-modal low here is somewhat higher than for all the

data, occurring in the interval between 25 and 30 percent porosity. Figure 10 is the corresponding histogram for the three-drill-hole composite conditioning data set, and it too reveals the bimodal welded/nonwelded distribution. A sharp frequency-low occurs at 25 percent porosity.

Figure 6 provides additional insight into the discrimination of welded from nonwelded rock types through use of a threshold porosity criterion. From this diagram, in which the porosity data can be viewed from their broader context of the thermal/mechanical units, it is clear that a threshold value of slightly more than 20-porosity percent separates the majority of samples taken from units containing a "w" in their designated abbreviation from those containing an "n."

Because of conceptual difficulties involved in considering materials of near-30-percent porosity as "welded," we opted for a criterion on the low side of the observed frequency minima. The conversion to thermal conductivity thus utilized a threshold value of 22.5 percent porosity for selecting the appropriate value of coefficient C_3 from table 1. If a grid node was simulated with a porosity less than or equal to 22.5 percent, the rock at that location was assumed to be welded and coefficients for equation (2) appropriate for welded materials were selected. If the value was greater than 22.5 percent, the rock was assumed to be nonwelded and the porosity value was converted accordingly.

Conversion from Stratigraphic to Real-World Coordinates

The geostatistical simulations were created in stratigraphic coordinates (fig. 4) and this coordinate system must be converted to actual, real-world coordinates prior to mapping the material properties onto finite-element meshes for use in thermal modeling. Offset of the various material-property units caused by post-depositional faulting (fig. 2) is accomplished through this coordinate conversion process as well. This use of an unfaulted geometry in modeling rock properties is consistent with a geologic interpretation that the material properties of the rock mass formed prior to tectonic disruption of the Yucca Mountain region.

The stratigraphic coordinate system used for the geostatistical modeling is represented schematically in figure 4. To produce the known eastward dip of the material property units and the fault offsets indicated by figure 2 and still be compatible with the requirements of the finite-element mesh used in the thermal calculations (Longenbaugh and others, 1995), a pixel-oriented transformation was required (fig. 11). This approach maintains all grid nodes within the model at a constant row-by-row elevation. Dipping beds are represented by a series of short, horizontal segments, each offset vertically relative to its neighbors by one or two pixels (fig. 11). A repetitive sequence of similar small offsets conveys the impression of tilted stratiform units while still allowing the direct mapping of the material-properties grid onto the equivalent finite-element mesh. In a similar manner, faulting was simplified to representation by major vertical offsets of the entire stratigraphic grid (fig. 11) at the surface location of the fault as digitized from figure 2. Faults at Yucca Mountain generally dip steeply at angles in excess of 70° (e.g., Scott and Bonk, 1984; Ortiz and others, 1985).

To allow for the cumulative displacement of the original grid, which occurs as the sum of numerous, small dip-inducing offsets and a few large-magnitude fault offsets, a buffer region of previously undefined grid nodes was added to the final grid (fig. 11). The buffer region was defined to leave a minimum five-grid-node zone around the offset original grid. These grid nodes were arbitrarily

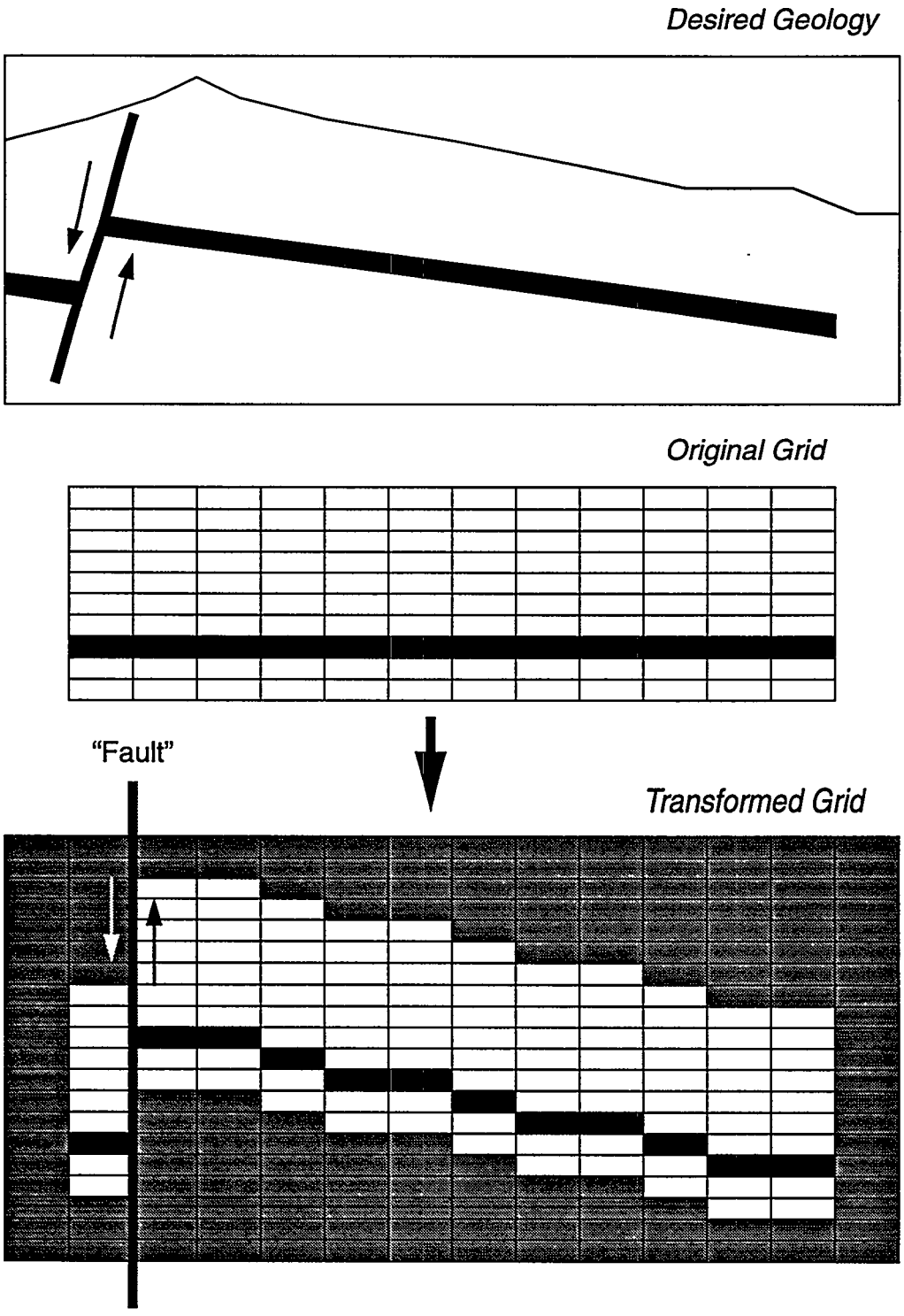

Figure 11. Schematic representation of the transformation process used to convert stratigraphic-grid coordinates (fig. 4) to real-world coordinates, thus capturing both dipping stratiform material-property units and fault offsets. Buffer cells (shaded) are added to ensure a complete rectangular grid after transformation.

assigned a material-property value that generally corresponded to a modal value as interpreted from the appropriate histogram. The actual value assigned is virtually irrelevant to the ultimate thermal calculations (Longenbaugh and others, 1995), because these nodes fall in the far-field portion of the computations. The finite-element mesh and underlying geostatistical models have been constructed such that the entire transient thermal pulse under investigation is contained within the near-field portion of the models.

Results

The results of constructing a number of models of material properties are presented and evaluated in this section. The final, most meaningful "evaluation" of these models using a numerical heat-conduction code is beyond the scope of this report (see Longenbaugh and others, 1995). However, this section discusses the reasonableness of the material-properties models from the perspective of the conceptual framework of Yucca Mountain, reproduction of appropriate statistical measures of the conditioning data used to generate the models, and the "realism" of the actual conditioning data themselves. Most discussion focuses on the specific models that were developed for numerical process modeling†. Other models have been created and are included in this report to illustrate particular aspects of the geostatistical modeling process or to suggest important aspects of the geology on which to focus in future thermal modeling work.

† Note added in proof: Originally three models, as discussed sequentially in this section, were developed for input to thermal analyses. Eventually, those initial analyses focused on only one geostatistical model, GC1HL, and several non-geostatistical material-property representations. These results are presented in Longenbaugh and others (1995). The other two named analyses from this report, GC2HL and GC3HL, plus additional geostatistical models, now have been evaluated using **COYOTE-II**, and the results are being prepared for publication.

Model GC1HL

Plate 1 presents a more-or-less baseline, simulated material-property model for porosity, bulk density, and thermal conductivity; it is identified as model GC1HL to correspond to the equivalent thermal calculation reported in Longenbaugh and others (1995). The model uses a 5,000-m range of spatial correlation and the single, composite-drill-hole set of conditioning data. A statistical summary of the model is given in table 3, and the histograms of the several material properties are presented as figure 12.

Table 3: Statistical Summary of Geostatistical Model GC1HL (Longenbaugh and others, 1995)
[Std.Dev. - standard deviation; C.V. - coefficient of variation, defined as the standard deviation divided by the mean]

	Measured	Simulated Model		
	Porosity Data (fraction)	Porosity (fraction)	Bulk Density (g/cm^3)	Thermal Conductivity (W/m-K)
Mean	0.19	0.17	1.91	1.593
Std. Dev.	0.11	0.08	0.20	0.310
C.V.	57%	47%	10%	19%
Maximum	0.65	0.65	2.31	2.128
Median	0.16	0.16	1.86	1.68
Minimum	0.02	0.02	0.79	0.252

As intended by selection of the data and geostatistical parameters used in the simulation, this model does an excellent job in capturing the layered conceptual model of Yucca Mountain. The material properties are well-layered, and the appropriate thermal/mechanical stratigraphic names are easily associated with those layers within the majority of the modeled region. These designations have been indicated on plate 1. The layered nature of the model breaks down somewhat in the lower one-third of the cross section. However, this is the far-field region of the thermal calculations, and, as suggested by figure 6, the available, measured porosity data are less-conclusively

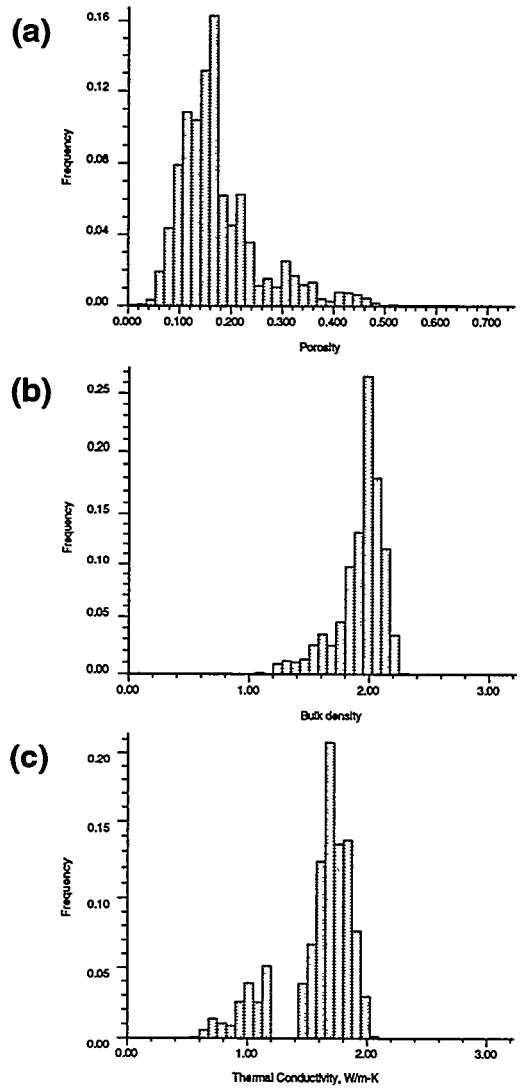

Figure 12. Histograms of (a) porosity, (b) bulk density, and (c) thermal conductivity values corresponding to geostatistical model GC1HL of Longenbaugh and others (1995).

segregated into layers in this portion of the geologic section. Faulted versions of the stratigraphic-coordinate models are presented in plate 2.

Statistically, the simulated model appears to be a reasonable reproduction of the conditioning data, as suggested by the comparison of the porosity statistics in table 3. Modeled porosity is somewhat less variable than the conditioning data (i.e., has a smaller coefficient of variation). However, as the correlation length used for the model (5,000 m) is greater than the horizontal extent of the cross section (slightly more than 3,000 m), this reduction in variability is not unexpected. This overall distribution of porosity values, as shown by the histogram of figure 12(a), adequately captures the bimodal, welded/nonwelded character of the data (compare to fig. 8(b)). The bimodal character of the model has been accentuated for the thermal conductivity values (fig. 12(c), because of the different coefficients used in the transformation of equation (2).

Vertical profiles of porosity values extracted from the model at several locations are shown in figure 13 for comparison with the input conditioning data. Note that in figure 13(a), which corresponds approximately to the actual location of the conditioning data used to represent drillhole USW G-4, the match of simulated porosity to the underlying composite drillhole data is quite good. The simulated values are generated only at the exact grid nodes specified in figure 4, whereas the irregularly spaced conditioning data are shown at their original sampled locations. Discrepancies between the conditioning data and the simulated porosity values can be attributed to the fact that exact collocation of the two types of information is only fortuitous. Figure 13(b) corresponds to a vertical profile located approximately 315 meters east of drillhole USW G-4. Because these simulated values are well constrained by data at the locations of both G-4 and drillhole UE-25 a#1, located an additional 700 meters to the east, the profile strongly resembles that extracted from the G-4 location. The same porosity units are easily identifiable. In contrast, figure 13(c) corresponds to a vertical profile extracted from the extreme western edge of the model. Located about as far from conditioning data as is possible, the resemblance to the G-4 conditioning data set is markedly less. The layered geologic system is still reproduced; however, the differences between porosity units are somewhat

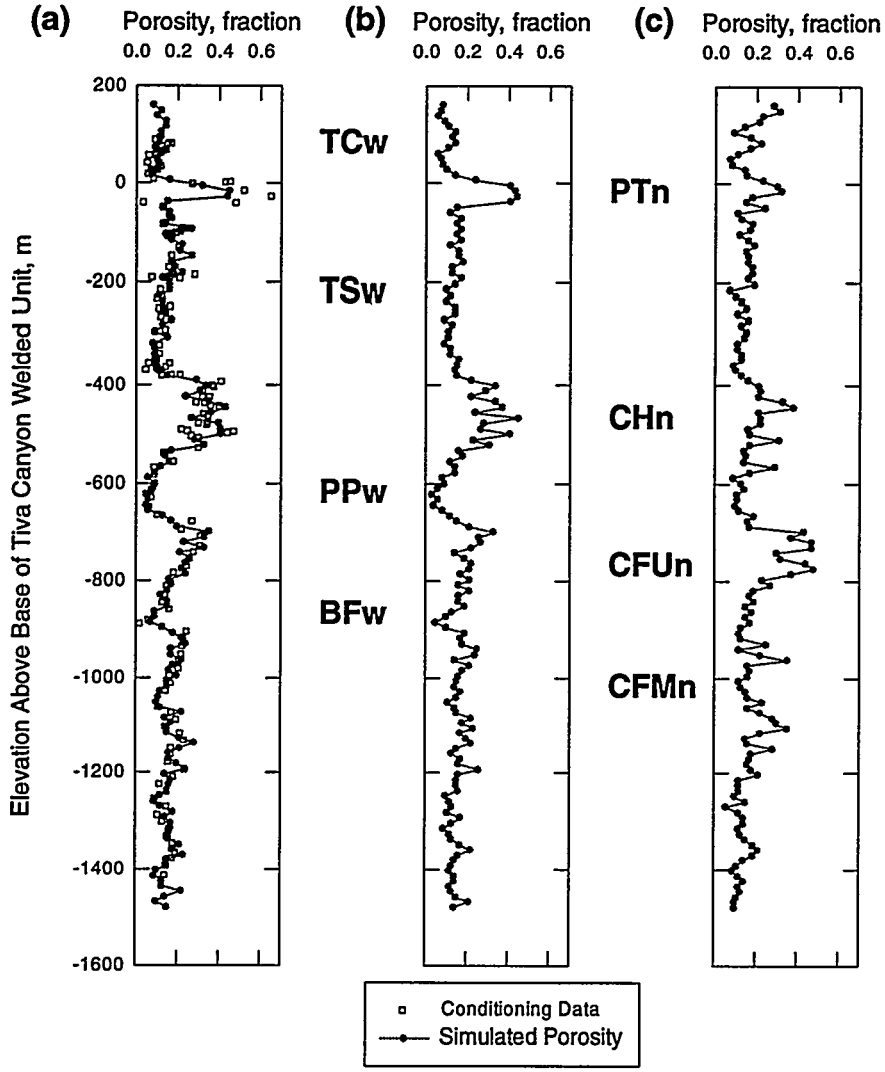

Figure 13. Vertical profiles of simulated porosity values extracted from model GC1HL at locations of (a) drillhole USW G-4; (b) *X*-coordinate 3378.25; and (c) *X*-coordinate 1015.75. Welded and nonwelded porosity units indicated; symbols correspond to usage of figure 3.

diminished in this ill-conditioned portion of the model.

Model GC2HL

For comparison, plate 3 presents the results for the same properties (in stratigraphic coordinates) of a simulated material-property model, referred to as model GC2HL, in which the range of spatial correlation has been reduced by a factor of one-fifth, to 1,000 m. The same conditioning data used in constructing model GC1HL, the replicated single composite drill hole, have been used in the construction of this model. The model is summarized statistically in table 4, and the histograms of the several material properties are presented in figure 14. The corresponding faulted version of this mode is shown in

Table 4: Statistical Summary of Geostatistical Model GC2HL

[Std.Dev. - standard deviation; C.V. - coefficient of variation, defined as the standard deviation divided by the mean]

	Measured	Simulated Model		
	Porosity Data (fraction)	Porosity (fraction)	Bulk Density (g/cm^3)	Thermal Conductivity (W/m-K)
Mean	0.19	0.15	1.91	1.584
Std. Dev.	0.11	0.10	0.25	0.327
C.V.	57%	56%	13%	20.7%
Maximum	0.65	0.68	2.33	2.164
Median	0.16	0.16	1.97	1.694
Minimum	0.02	0.02	0.73	0.210

plate 4. Vertical porosity profiles similar to figure 13 are not presented for this model.

The effect of the shorter range of spatial correlation is immediately apparent in plate 3, and, to a slightly greater extent because of the additional visual disruption due to post-processing, in plate 4. Although the gross layering, corresponding to the major thermal/mechanical units, of the model is maintained, comparison with plate 1 indicates that the specific values of the various properties form more discontinuous lozenge-like shapes. For the deeper stratigraphic units, the blurring of the major unit "contacts" is more pronounced than for the distinction between the Paintbrush nonwelded unit (PTn) and its adjacent densely welded neighbors, TCw and TSw. The contrasts in value of the conditioning data simply are not as great in the lower units, and these limited contrasts cannot be propagated away from the conditioning drill holes with the same "confidence" as with the longer range of spatial correlation.

Statistically, the simulated model captures the nature of the conditioning data set quite adequately. table 4 indicates a close match for the various statistical measures in the two porosity columns. Note that even the coefficient of variation is more similar for the

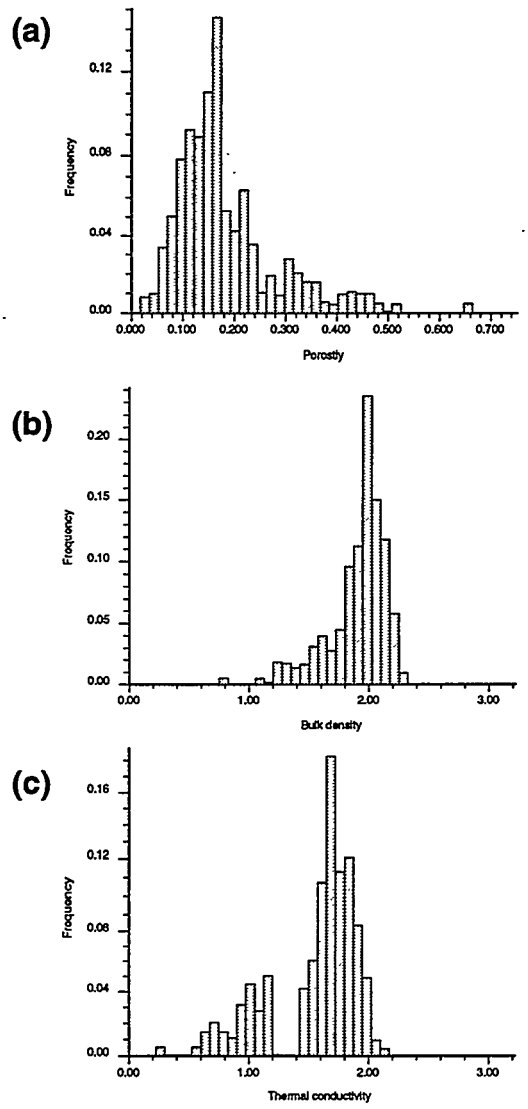

Figure 14. Histograms of (a) porosity, (b) bulk density, and (c) thermal conductivity values corresponding to geostatistical model GC2HL.

less-strongly spatially correlated model, than it was for model GC1HL. The histogram of the simulated model (fig. 14(a)) is appropriately bimodal, and approximates that of the conditioning data (fig. 8(b)).

Model GC3HL

More geologically realistic models of material properties may be generated by using the most realistic data possible to condition the simulation algorithm. Rather than simply produce an "ideally" layered physical-property

model by replicating a single conditioning drill hole, model GC3HL, portrayed in plate 5, attempts to capture the actual level of lateral variability present at Yucca Mountain by using spatially variable drill hole information projected onto the modeled plane of cross section. Statistical summary measures of porosity, bulk density, and thermal conductivity for this model are given in table 5; histograms of the simulated model are presented as figure 15. Vertical porosity profiles corresponding to the input three-drill-hole composite data set are presented in figure 16, parts (a) through (c).

Table 5: Statistical Summary of Geostatistical Model GC3HL

[Std.Dev. - standard deviation; C.V. - coefficient of variation, defined as the standard deviation divided by the mean]

	Measured	Simulated Model		
	Porosity Data (fraction)	Porosity (fraction)	Bulk Density (g/cm^3)	Thermal Conductivity (W/m-K)
Mean	0.20	0.17	1.93	1.584
Std. Dev.	0.16	0.08	0.20	0.327
C.V.	57%	48%	10%	20.7%
Maximum	0.65	0.67	2.32	2.164
Median	0.17	0.15	1.99	1.694
Minimum	0.01	0.01	0.75	0.210

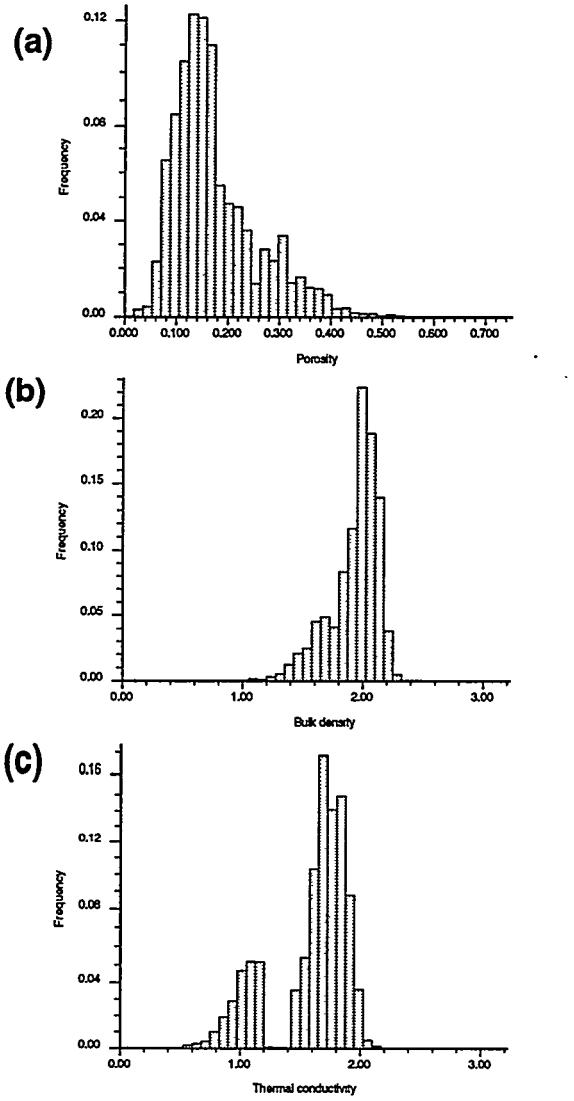

Figure 15. Histograms of (a) porosity, (b) bulk density, and (c) thermal conductivity values corresponding to geostatistical model GC3HL.

This model, as portrayed in stratigraphic coordinates in plate 5 and, in its faulted version in plate 6, represents a return to the well-layered conceptual model, as required by the input 5,000-m spatial-correlation length. However, the figure indicates a somewhat less-strikingly laminated model than that of plate 1. These differences can be traced to variations in the data used to condition the two models. Specifically, whereas model GC1HL (plate 1) used the identical composite drill hole, replicated in three locations along the cross section, model GC3HL (plate 5) uses three different composite drill holes at the same physical locations. Horizontal variability in the values of the conditioning porosity data thus propagates away from the drill-hole locations and does influence the appearance of the model. Both "unit" thicknesses and property magnitudes are affected. Reproduction of the conditioning porosity profiles at the actual drill hole locations (figs. 16(a) to (c)), however, is generally excellent.

There are two notable examples of this type of horizontal variability. The first exam-

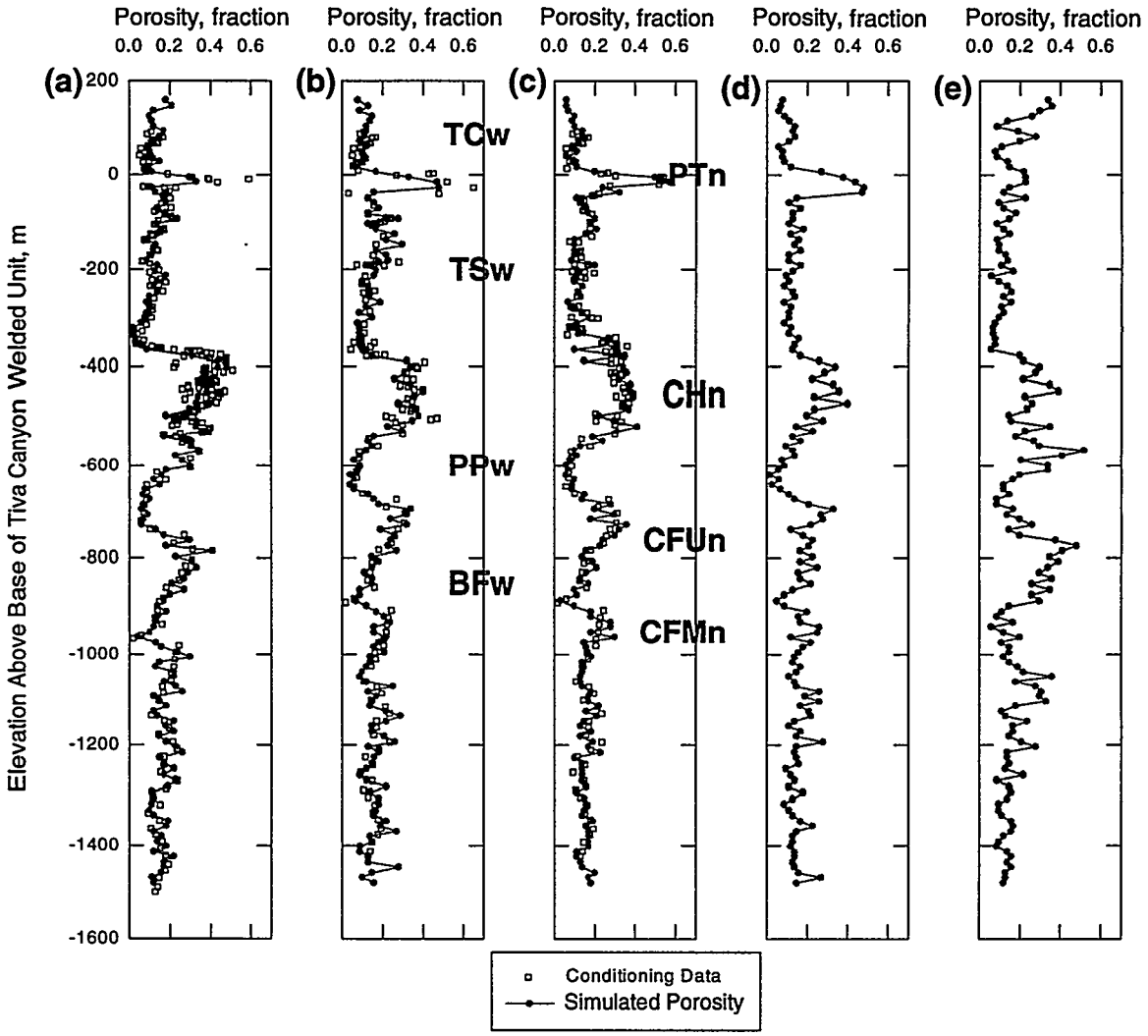

Figure 16. Vertical profiles of simulated porosity values extracted from model GC3HL at locations of (a) drillhole USW GU-3/G-3; (b) drillhole USW G-4; (c) drillhole UE-25 a#1; *X*-coordinate 3378.25; and (e) *X*-coordinate 1015.75. Welded and nonwelded porosity units indicated; symbols correspond to usage of figure 3.

ple involves the high-porosity layer near the top of the model, corresponding to the Paintbrush nonwelded (PTn) thermal/mechanical unit. Referring to the three drill holes used to condition this model, shown in figure 9 (right-hand three columns) and also shown superimposed on the simulated values in figure 16, we see that the average porosity value contained within the PTn unit is definitely higher in drill hole USW G-4 (the maximum value appears to exceed 60 percent) than in the other two holes. The color-coded porosity in this layer in plate 5 indicates higher porosities in the slightly-right-of-center portion of the model, which corresponds to the projected physical location of USW G-4. In contrast, the average porosity in the PTn unit in hole USW GU-3/G-3 (thickness adjusted) is noticeable lower than in the other drill holes. Only one sample approximates 60-percent porosity, and there seem to be three or four values in the 30 to 40-percent porosity range. These conditioning data propa-

gate into the lower simulated porosity values visible on the left-hand (west) side of plate 5. The simulated porosity values at the drill hole locations are not quite generally as large as the maximum of the conditioning data (fig. 16); this is interpreted as a consequence of the relevant grid nodes being influenced by multiple samples of lower average value.

The second example of lateral variability involves the lowermost portion of the Topopah Spring welded unit (TSw3 of Ortiz and others, 1985; fig. 3). Again referring to figures 9 and 16, we can see that the lowest porosity values represented on the entire figure are located at the base of the TSw unit in drill hole USW GU-3/G-3 (immediately above the lower arrow indicating the thickness adjustment in fig. 9). This numerical representation of the low-porosity vitrophyre of the TSw3 unit is quantitatively different from the equivalent numerical representation in drill hole USW G-4, and particularly in hole UE-25 a#1. These differences in conditioning data for thermal/mechanical unit TSw3 propagate through the simulation algorithm, and are reflected in the difference in color-coded porosity values immediately above the higher-porosity zone corresponding to the CHn nonwelded interval. Lower porosities (darker colors) occur on the left-hand side of plate 5 at this stratigraphic position.

Lateral heterogeneity can also be observed in the vertical profiles of figure 16. The vertical porosity profiles of figure 16(d) and (e) have been extracted from two locations that do not correspond to conditioning drill hole information. The profile of figure 16(d) is located approximately 315 meters east of drillhole USW G-4 (compare to fig. 13(b)) and reflects the strong influence of nearby conditioning drill hole information in both directions. Figure 16(e) (compare to fig. 13(c)), located at the extreme west margin of the model domain, was selected to represent the least-well conditioned portion of the model. Note that reproduction of alternating high and low porosity units in the upper part of the model is less well developed than in figure 16(d). However, a very low porosity interval corresponding to the Topopah Spring lower vitrophyre (TSw3) conditioning data in drill hole USW GU-3/G-3 is present, indicating that conditioning information is propagating to this extreme margin of the model.

Effect of Spatial Correlation Length

Although comparing models GC1HL and GC2HL provides a brief examination of the effect of spatial correlation length, or range of the variogram, on the resulting geostatistical material-properties model, a more comprehensive examination of the effect of this parameter was conducted. Plate 7 presents a comparison of five models with correlation lengths varying from 10,000 m to 500 m. The identical, single-composite-drill-hole data have been used to condition each model. Other modeling parameters are identical, and only the range of correlation is different.

The models constructed using spatial correlation lengths of 10,000 m (plate 7(a)) and 5,000 m (plate 7(b)) appear visually identical. Major material-property units extend completely across the modeled cross section, and even the distribution of simulated porosity values within those units appears virtually identical. This result is not particularly surprising, because the complete lateral extent of the modeled cross section is slightly in excess of 3,100 m, and the specified input ranges of correlation exceed this distance. The conditioning data are expanded away from their locations in effectively the same manner as a consequence. Even the random paths defined through the grid are identical in these two models because they both use the same random-number seed.

For the model constructed using the 2,000 m range of spatial correlation (plate

7(c)), the major property units have been propagated quite reasonably across the entire model domain. This spatial correlation length is approximately two-thirds the horizontal extent of the cross section. However, there are obvious differences in the distribution of specific ranges of porosity values within those units. The origin of these differences is not entirely obvious. Although the spatial correlation length is shorter than the entire extent of the model domain, that 2,000 m length is more than sufficient to link at least two of the three replicated conditioning "drill holes." Because all other simulation parameters were identical (including the random path through the grid), we tentatively interpret the variation in porosity values as originating from the fact that the stated anisotropy ratio was kept constant at 20:1 (horizontal:vertical). As the horizontal correlation length varies, the effective vertical correlation length will change proportionately. Thus, although conditioning data located precisely along the major axis of the variogram ellipse will enter the simulation in an identical manner, the relative weights assigned to conditioning values at slight angles to that major axis will be different. The estimated position of the unsampled location on the porosity ccdf is thus different, and the simulated value, which results from sampling that ccdf, will differ as well. That this effect is, indeed, occurring is suggested by the observation that the identically color-coded lenses within a particular material properties unit appear thicker in plate 7(c) than equivalent lenses in plate 7(a) and (b).

The models generated using a range of spatial correlation of 1,000 m (plate 7(d)) and 500 m (plate 7(e)) exhibit a progressive breakdown of the material property units conceptually expected in a model of Yucca Mountain. There is a suggestion of through-going property units in plate 7(d), but this model is no longer "well-layered." The model of plate 7(e) is layered, but the layering is now "stochastic" in nature, as the 500-m range of correlation is less than the inter-drill-hole distance.

Effect of Assumed Initial Saturation

As discussed under the section on "Porosity Surrogate for Thermal Conductivity" on page 8, most of the models created for this study assumed a uniform, "representative," 60-percent initial moisture saturation for purposes of converting porosity to thermal conductivity via equation (2). Yet as suggested by the saturation profile of figure 5, the actual saturations of welded and nonwelded materials are, in fact, likely to be different. To investigate the sensitivity of the resulting material-property models of thermal conductivity to the initial saturation level assumed for the variable transformation, the porosity models were converted to thermal conductivity at assumed saturations of 80 percent for welded materials and 40 percent for nonwelded. These values capture some of the essence of figure 5, which indicates that welded materials are significantly more saturated than nonwelded tuffs. The values of 80 percent and 40 percent are approximately the average saturations observed in the near-field thermal mechanical units of the TSw and PTn. Saturations exceed 80 percent in the lower part of the TSw thermal/mechanical unit. Variable conversion was carried out at a constant initial temperature of 50°C.

Figure 17 compares the results of these conversions at different saturations through the effects on the histogram of thermal conductivity values for models generated from the most-geologically realistic three-drill-hole composite conditioning data. Although the differences are somewhat subtle, the increased "spread" in saturation between welded and nonwelded rock types in the second version of the model has increased the separation of the two modes of thermal conductivity values on the histograms. In figure 17(a), which represents the

thermal conductivities converted at a uniform 60-percent saturation for both welded and nonwelded materials, there is an essentially unpopulated break between the two populations of 0.2 W/m-K. In figure 17(b), which corresponds to the 80-/40-percent saturation conversion, this unpopulated gap has nearly doubled to 0.4 W/m-K. Referring to the saturation profile shown in figure 5, the difference in saturation between welded and nonwelded lithologies may be as much as the difference between greater than 90 percent and less than 20 percent. In such extreme actual cases, it would appear that the differences in thermal conductivity between these two rock classifications would be accentuated.

Although the influence of these types of differences in thermal conductivity on the ultimate temperature profiles has not been investigated as part of this study, it would appear that it may be preferable to account for saturation in a more sophisticated manner than has been done here. Naturally enough, it is the near-field region of a thermal calculation that exerts the greatest influence on the modeled temperature regime. Thus conversion of surrogate porosity models to represent thermal conductivity should represent the actual saturations prevailing in the near-field region to the extent possible. Thermal models similar to that of Longenbaugh and others (1995) could be used to suggest the likely vertical extent of the near-field region for use in examining available saturation data to use in the conversion relationship (equation (2)). Saturation values more representative of this specific vertical interval could then be used in equation (2). Although not possible with the limited data currently available, the closer approximation to reality would be to use only porosity data for which there are corresponding in-situ saturation data, such as exist for drill hole UE-25 UZ-16 (fig. 5). These porosity measurements could be converted to thermal conductivity at nearly "true" initial saturations, and the resulting pseudo thermal conductivity values used to simulate thermal conductivity fields directly, instead of converting a simulated porosity field.

Effect of Assumed Initial Temperature

The thermal conductivity models created for use in thermal-process modeling were converted from spatially correlated porosity fields at an initial temperature of 50°C, which was believed to be an approximately correct

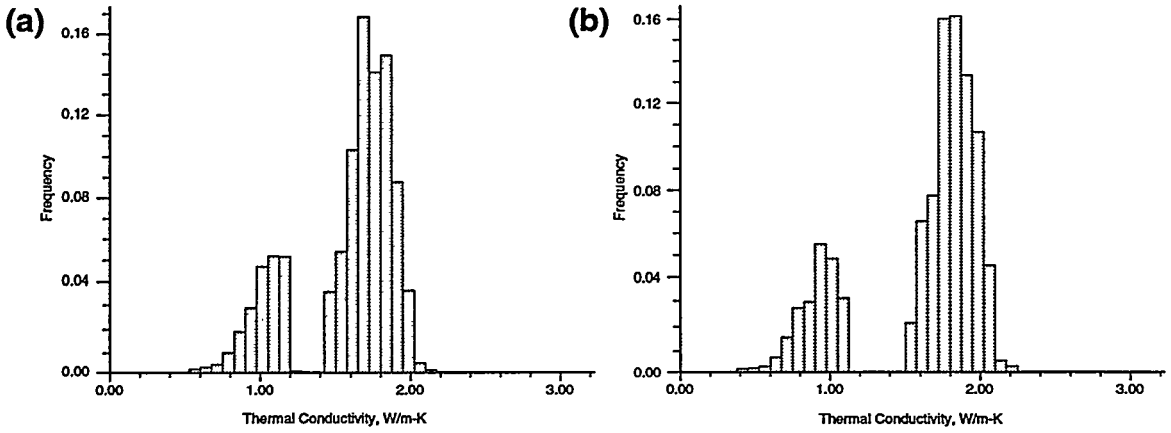

Figure 17. Histograms of thermal conductivity models for which the conversion from porosity to thermal conductivity was made at (a) uniform saturations of 60 percent and (b) 80 percent for welded tuff and 40 percent for nonwelded materials. Three-drill-hole composite data, 5,000 m correlation length.

in-situ temperature; 50°C is also the median temperature at which the original laboratory measurement of thermal conductivity was carried out. Because the conversion relationship of equation (2) contains a dependency on temperature, several additional models have been created at different initial temperatures. Figure 18 illustrates histograms of thermal conductivity models created at three temperatures: 50°C, representing near-in-situ initial, sub-boiling conditions for pore water; 100°C, representing near-boiling to boiling conditions; and 110°C, which presumably represents the thermal conductivity contrasts that might prevail after dry-out of the potential repository volume by sustained heating.

From the evidence in figure 18, it appears that increasing the initial temperature assumed for converting porosity to thermal conductivity first increases the effective conductivity values without much effect on the relative proportion of different values within each rock type. Once the transition to near-boiling temperatures has dried out the rock, however, the thermal conductivity of both welded and nonwelded lithologies appears to decrease markedly, reflecting more efficient heat conduction via the contained pore water than by the rock matrix. Convection of pore fluids is not considered by the COYOTE-II computer code (Longenbaugh and others, 1995). For the models represented by figures 18(b) and 18(c), there is a decrease of approximately 30-35 percent in the modal conductivity of each rock type. Preliminary investigation of the effects of thermal conductivity values that vary as a function of temperature has been conducted for non-geostatistical material-property fields by Longenbaugh and others (1995) using temperature functions from Lawrence Livermore National Laboratory (TRW, 1994). These same techniques have been applied to spatially correlated, heterogeneous property fields, and the results are in preparation (see footnote on page 21).

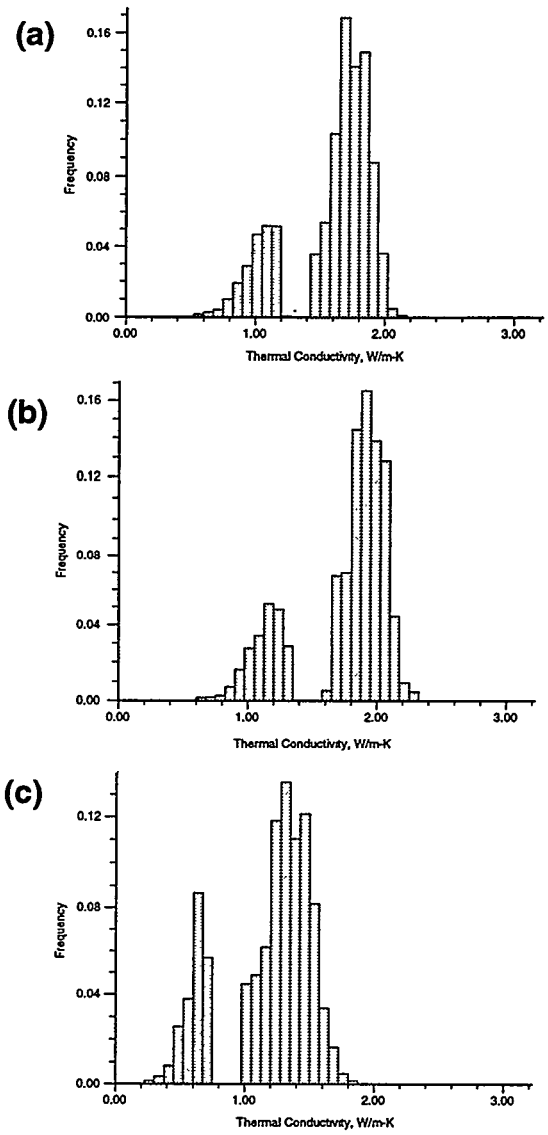

Figure 18. Histograms of thermal conductivity models converted from porosity simulations at (a) 50°C, (b) 100°C, and (c) 110°C. Three-drill-hole composite porosity data; correlation length 5,000 m.

Uncertainty Considerations

Although the assessment of the geologic uncertainty resulting from less-than-exhaustive site characterization was not an objective of this modeling study, it is instructive to consider the potential simulation-to-simulation variability that is likely using this approach. This discussion of geologic uncertainty focuses only on the surrogate porosity models, and does not address the additional

uncertainty that is introduced through the porosity-to-thermal conductivity transformation of equation (2).

Figure 19, panels (a) though (d), presents four randomly selected, individual simulations of porosity for the single-composite-drill-hole data set, generated using a spatial correlation length of 5,000 m (compare to plate 1). The well-layered nature of the simulation is evident, and the individual welded and nonwelded material property units are identifiable and continuous. There is a small degree of variability among the four models; however, the visual appearance and the statistical properties of the various realizations, or stochastic images, is sufficiently similar that they are, in effect, indistinguishable except for the random-number seed used to begin the simulation process.

Figure 19 (e), in contrast, is an "expected-value" profile, constructed by averaging ten separate simulations (including the four of panels (a) through (d)) on a pixel-by-pixel basis and displaying the grey-scale-coded mean (expected) value. This expected-value profile corresponds in theory to the more-conventional kriged (estimated) model. In this summary image, or alternative model, the local variability evident in the individual, equally likely realizations Figure 19 (a) through (d) has been averaged-out, and the

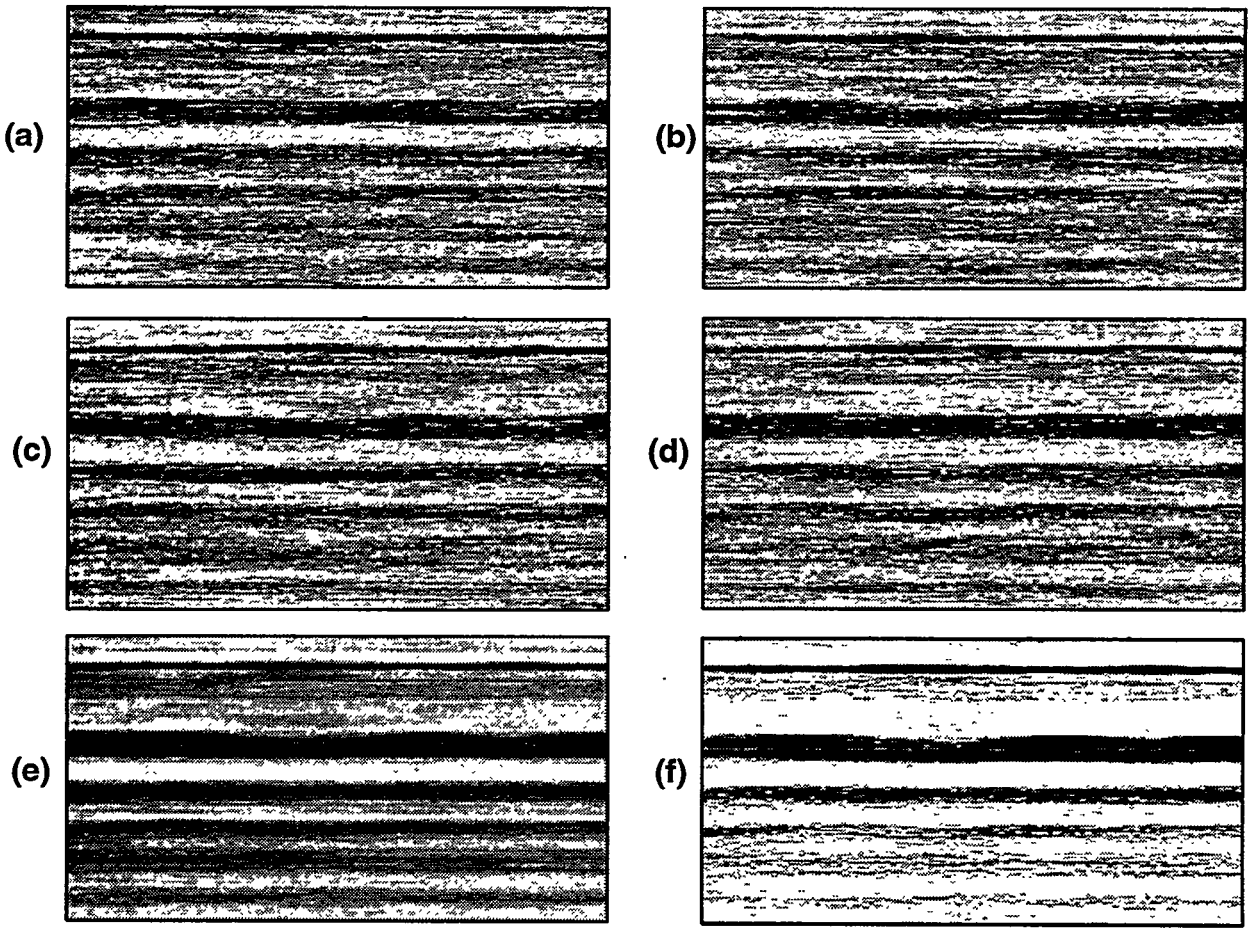

Figure 19. (a) to (d): Grey-scale coded images of four randomly selected porosity simulations; range of spatial correlation 5,000 m. (e): Expected value image of porosity constructed from ten simulations. Porosity values coded from 0 (white) to >0.4 (black). (f) Probability image for $Pr(\phi > 0.225)$. Probability scale runs from 0 (white) to 1 (black).

various material-property units appear even more smooth and continuous.

Figure 19 (f) represents an entirely different method of visualizing the geology of the cross section. In this image, the individual pixels no longer represent porosity values, but rather they portray the *probability* that the porosity at the corresponding location exceeds 22.5 percent, which was used to determine the break between welded and nonwelded materials for purposes of converting porosity to thermal conductivity (see "Discrimination of Welded from Nonwelded Rock Type" on page 18). This probability is grey-scale coded from zero (extremely unlikely to exceed 0.225 = welded) to one (almost certain to exceed 0.225 = nonwelded). The probability value is approximated by examining a set of simulations and counting the proportion of those alternative realizations that exceed the desired threshold value. For this particular version of the geostatistical models of Yucca Mountain, there is relatively little uncertainty. Much of figure 19 (f) is either very dark or nearly white, corresponding to near-certainty in the lithology. Uncertainty, indicated by median (50:50 probability) grey-coded values, is largest in the lower part of the cross section, where the conditioning porosity data themselves are somewhat equivocal, and in the upper portion of the Topopah Spring welded (TSw) unit, where matrix porosities are somewhat higher than usual due to more-intense vapor-phase alteration.

In marked contrast to figure 19, the degree of geologic uncertainty indicated for the single-composite drill hole model constructed using a spatial correlation length of only 1,000 m is significantly greater. Four randomly selected, alternative simulations are presented in figure 20 (a) through (d) (compare with plate 3). The expected-value profile and probability profile are shown in figure 20 (e) and (f).

For this set of simulated models, the well-layered, conceptual geologic model is best visualized "on average," as represented by the expected-value profile (fig. 20(e)). However, the actual distribution of porosity values in reality may be quite different from that expectation, as indicated by the variability of the individual realizations. *Statistically*, the realizations are virtually indistinguishable from one another and from the known data. If the problem being evaluated is *location-specific*, the *implications* of the various equally likely simulated models may be quite different.

The increased uncertainty inherent in this less-strongly correlated model of Yucca Mountain is well reflected in the probability profile of figure 20(f). In distinct contrast to the equivalent image in figure 19, most of figure 20(f) is relatively grey, indicating probabilities significantly different from zero or one. Uncertainty changes laterally within the material-property units. Note that the regions of most intense black and white occur vertically above one another, and that this pattern of intense black and white occurs at three locations across the cross section. These are the locations of the three replications of the single-composite drill hole porosity profile used to condition the model; near the data, there is little uncertainty.

The difference between simulated models and the corresponding expected-value summary (or kriged type of model) is emphasized through figure 21, which presents the complete univariate distribution (i.e., histogram) of porosity values for the two expected-value models of figures 19 and 20. Histograms of corresponding simulated models are presented in figure 12(a) and 14(a). Although the bimodal, welded/nonwelded nature of Yucca Mountain geology is preserved at a somewhat subdued level in figure 21(a), that bimodality is almost completely extinguished through the "averaging" process in figure 21(b). Indeed,

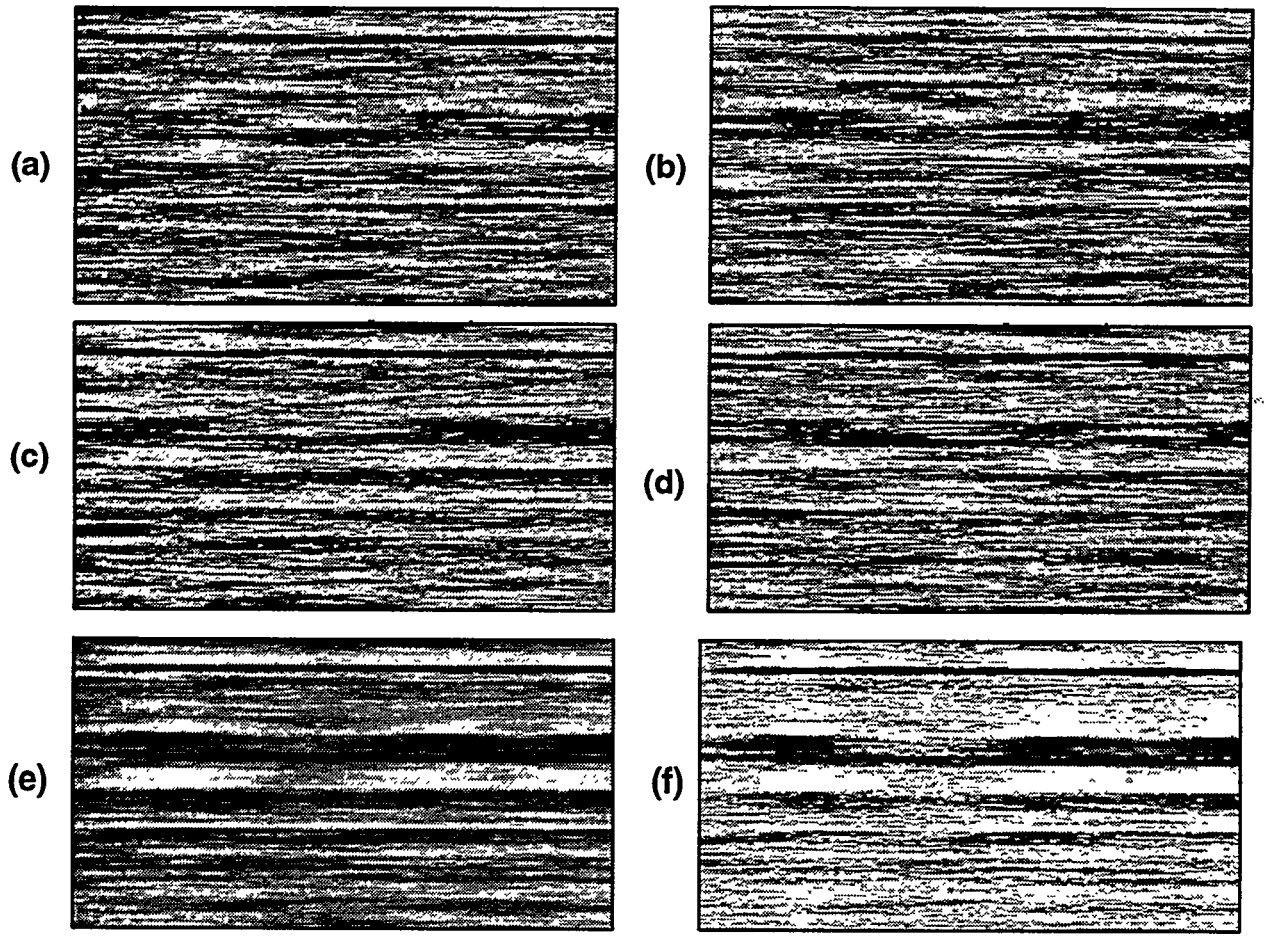

Figure 20. (a) to (d): Grey-scale coded images of four randomly selected simulations of porosity, range of spatial correlation 1,000 m. (e): Expected value image of porosity constructed from ten simulations. Porosity values coded from 0 (white) to >0.4 (black). (f) Probability image for Pr(ϕ > 0.225). Probability scale runs from 0 (white) to 1 (black).

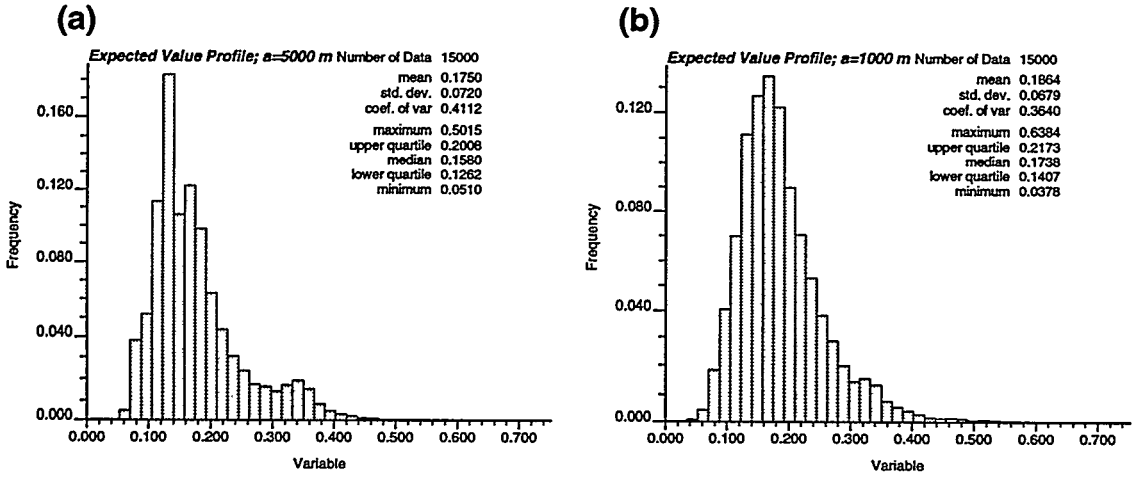

Figure 21. Histograms of expected-value profiles corresponding to (a) figure 19(e), range of spatial correlation 5,000 m and (b) figure 20(e), range of spatial correlation 1,000 m (note change in axis scale).

the distribution of figure 21(b) exhibits a pronounced Gaussian appearance, despite the fact that the original data from which the model was constructed were distinctly non-Gaussian. In both expected-value profiles, the extreme tail of the distribution is virtually gone, with only a very small proportion of the modeled values exceeding 40-percent porosity. If the physical process of concern is sensitive to these extreme values, the performance implications of the two types of models may be quite different.

Conclusions

Two-dimensional, heterogeneous, spatially correlated models of thermal conductivity and bulk density have been created for a representative, east-west cross section of Yucca Mountain using geostatistical simulation. The models were created for use as input to finite-element heat-conduction analyses comparing different methods of representing spatial variability in material properties. The thermal conductivity models are derived from surrogate material-property models through multiple linear regression analyses that relate thermal conductivity to porosity as a function of temperature and initial saturation. Bulk density values were obtained through a similar, linear-regression relationship. The use of surrogate-property models allows the use of spatially much-more-abundant porosity measurements to condition the simulations. Modeling was conducted in stratigraphic coordinates to represent original depositional continuity of material properties. The completed models were transformed to real-world coordinates to capture present-day tectonic tilt and fault offset of the material-property units. Spatial correlation lengths required for geostatistical modeling were assumed, but are based on the results of previous transect-sampling and geostatistical-modeling work.

Two different sets of conditioning data have been used in the modeling of porosity and its thermal-conductivity equivalent. One set consists of a single, composite porosity profile, developed using segments of selected actual drill holes, which was replicated in three locations across the modeled cross section. This approach was taken specifically to generate a well-layered material-property system. The second set consisted of three different, composite porosity profiles corresponding approximately to three separate drill holes projected onto the plane of cross section, and was intended to generate models that represent lateral, as well as vertical, material-property heterogeneity.

The resulting models appear to be reasonable, quantitative representations of the relevant, spatially variable material-properties. Visually, the models recreate the conceptual image of Yucca Mountain as a layered system comprised of alternating units of welded and nonwelded tuff and related volcaniclastic materials. Layering is better-developed in the upper part of the models, corresponding to the several members of the Paintbrush Tuff, which consist of massive welded units separated by thinner nonwelded intervals. Layering is less well-developed in the lower part of the models, where contrasts in the degree of welding are known to be less prominent in the several members of the Crater Flat Tuff. For the three-drill-hole conditioning-data models, lateral variations are observed in material properties within individual material-property units; these lateral variations are consistent with the spatially variable conditioning porosity information.

Statistically, the completed material-property models appear very similar to the measured porosity data. Although the entire cross section of Yucca Mountain was simulated in one pass, the distribution of material-property values is appropriately bimodal, rep-

resenting the physical distinction between welded and nonwelded rock types. The degree of heterogeneity, as summarized by both histograms and descriptive statistics, appears appropriate and virtually identical to that of the input conditioning data. These models are essentially indistinguishable from the real-world observations. In contrast to the resemblance of the simulated models to the measured data, models showing the most likely material-property value prevailing at each spatial location (expected-value, or kriged, profiles) can be demonstrated to have statistical properties which are quite different from those of the original data. In particular, the degree of heterogeneity is reduced through the expected-value modeling process. If the physical process under investigation is sensitive to this loss of real-world heterogeneity and the presence of fewer tail values, the results of numerical modeling of that process using the two approaches to modeling material properties may be quite different and yield different conclusions.

A number of models have been created as preliminary sensitivity studies of assumed modeling parameters. Varying the spatial correlation length assumed for simulation over one-and-a-half orders of magnitude yielded predictable results; the layering induced in the spatially correlated models deteriorated to geologically unacceptable discontinuous lenses for ranges of correlation less than 1,000 m. The transformation of porosity to thermal conductivity via the observed multiple-regression relationship appears most sensitive to initial saturation. Welded and nonwelded rock types may exhibit significantly different in-situ saturations, and increasing the difference in saturation appears to widen the modal separation of thermal conductivity values for the two lithologies. Accurate representation of actual saturation levels appears to be important. Changes in the initial temperature assumed for converting porosity to thermal conductivity changes the absolute magnitude of the resulting thermal-conductivity values; however the relative difference in conductivity appears relatively insensitive to temperature of conversion.

References

Anderson, L.A., 1981, Rock property analysis of core samples from the Yucca Mountain UE-25 a#1 borehole, Nevada Test Site, Nevada: U.S. Geological Survey Open-File Report 81-1338, 40 p.

Anderson, L.A., 1984, Rock property measurements on large-volume core samples from Yucca Mountain USW GU-3/G-3 and USW G-4 boreholes, Nevada Test Site, Nevada: U.S. Geological Survey Open-File Report 84-552, 42 p.

ASTM [American Society for Testing and Materials], 1977, F433-77 (reapproved 1987) Standard practice for evaluating thermal conductivity of gasket materials: Annual book of ASTM standards, American Society for Testing and Materials, Philadelphia, Penna.

Brandshaug, T., 1991, A thermomechanical far-field model of Yucca Mountain: Sandia Report SAND85-7101, Sandia National Laboratories, Albuquerque, N.Mex., 120 p.

Buesch, D.C., Nelson, J.E., Dickerson, R.P., and Spengler, R.W., 1993, Development of 3-D lithostratigraphic models at Yucca Mountain, Nevada, *in* High-Level Radioactive Waste Management, Proceedings of the Fourth International Conference, LaGrange Park, Ill.: American Nuclear Society, p. 943-948.

Deutsch, C.V., and Journel, A.G., 1992, GSLIB geostatistical software library and user's guide, New York: Oxford University Press, 340 p.

Flint, L.E., and Flint, A.L., 1990. Preliminary permeability and water-retention data for nonwelded and bedded tuff samples, Yucca Mountain area, Nye County, Nevada: U.S.

Geological Survey Open-File Report 90-569, 172 p.

Gartling, D.K. and Hogan, R.E., 1994, COYOTE-II — A finite-element computer program for nonlinear heat conduction problems, Part I Theroretical background: Sandia Report SAND94-2274, Sandia National Laboratories, Albuquerque, N.Mex., 63 p.

Istok, J.D., Rautman, C.A., Flint, L.E., and Flint, A.L., 1994, Spatial variability in hydrologic properties of a volcanic tuff: Ground Water, v. 32, p. 751-760.

Journel, A.G., and Alabert, F., 1989, Non-Gaussian data expansion in the earth sciences: Terra Nova, v. 1, p. 123-134.

Journel, A.G., and Huijbregts, Ch.J., 1978, Mining geostatistics, New York: Academic Press, 600 p.

Knauss, K.G., Beiriger, W.J., Peifer, D.W., and Piwinskii, A.J. 1985. Hydrothermal interaction of solid wafers of Topopah Spring tuff with J-13 water and distilled water at 90, 150, and 250 C, using Dickson-type, gold-bag rocking autoclave, Report UCRL-53645, Lawrence Livermore National Laboratories, Livermore, CA.

Knauss, K.G., and Peifer, D.W., 1986. Reaction of vitric Topopah Spring tuff and J-13 Ground water under hydrothermal conditions using Dickson-type, gold-bag rocking autoclaves: Report UCRL-53795, Lawrence Livermore National Laboratories, Livermore, CA.

Lin, W., and Daily, W., 1984. Transport Properties of Topopah Spring tuff, Report UCRL-53602, Lawrence Livermore National Laboratories, Livermore, CA.

Longenbaugh, R., Rautman, C.A., and Ryder, E.E., 1995, Yucca Mountain thermal response: An evaluation of the effects of modeled geologic structure and thermal property descriptions: Sandia Report SAND94-2247. Sandia National Laboratories, Albuquerque, NM, 136 p.

Ortiz, T.S., Williams, R.L., Nimick, F.B., Whittet, B.C., and South, D.L., 1985, A three-dimensional model of reference thermal/mechanical and hydrological stratigraphy at Yucca Mountain, southern Nevada: Sandia Report SAND84-1076. Sandia National Laboratories, Albuquerque, NM, 76 p.

Peters, R.R., Klavetter, E.A., Hall, I.J., Blair, S.C., Heller, P.R., and Gee, G.W, 1984. Fracture and Matrix hydrogeologic characteristics of tuffaceous materials from Yucca Mountain, Nye County, Nevada, Sandia Report SAND84-1471, Sandia National Laboratories, Albuquerque, NM.

Rautman, C.A., 1991, Estimates of spatial correlation in volcanic tuff, Yucca Mountain, Nevada: Sandia Report SAND89-2270, Sandia National Laboratories, Albuquerque, N.Mex., 110 p.

Rautman, C.A., and Flint, A.L., 1992, Deterministic geologic processes and stochastic modeling, *in* High-Level Radioactive Waste Management, Proceedings of the Third International Conference, LaGrange Park, Ill.: American Nuclear Society, p. 1617-1624.

Rautman, C.A., and Robey, T.H., 1994, Development of stochastic indicator models of lithology, Yucca Mountain, Nevada, *in* High-Level Radioactive Waste Management, Proceedings of the Fifth International Conference, LaGrange Park, Ill.: American Nuclear Society, p. 2510-2519.

Rautman, C. A., Flint, A.L., Chornack, M.P., and McGraw, M.A. 1991, Microstratigraphic units and spatial correlation of hydrologic properties in tuff, Yucca Mountain, Nevada: Geological Society America, Abstracts with Programs, v. 23, no. 5, p. A119-120.

Rautman, C. A., Flint, L.E., Flint, A.L., and Istok, J.D., 1995, Physical and hydrologic properties of outcrop samples from a nonwelded to welded tuff transition, Yucca Mountain, Nevada: U. S. Geological Survey Water-Resources Investigations Report 95-4061, 28 p.

Robison, J.H., and Craig, R.W., 1991, Geohydrology of rocks penetrated by test well USW H-5, Yucca Mountain, Nevada: U.S. Geological Survey Water-Resources Investigation Report 88-4168, 44 p.

Rush, F.E., Thordarson, W., and Bruckheimer, L., 1983. Geohydrologic and drill-hole data for test well USW H-1, adjacent to the Nevada Test Site, Nye County, Nevada: U.S. Geological Survey Open-File Report 83-141, 44 p.

Schenker, A.R., Guerin, D.C., Robey, T.H., Rautman, C.A., and Barnard, R.W., 1995, Stochastic hydrogeologic units and hydrogeologic properties development for total system performance assessments: Sandia Report SAND94-0244, Sandia National Laboratories, Albuquerque, NM, 172 p.

Schwartz, B.M., 1990, SNL Yucca Mountain Project data report, density and porosity data for tuffs from the unsaturated zone at Yucca Mountain, Nevada: Sandia Report SAND88-0811, Sandia National Laboratories, Albuquerque, NM.

Scott, R.B. and Bonk, J., 1984, Preliminary geologic map of Yucca Mountain with geologic sections, Nye County, Nevada: U.S. Geological Survey Open-File Report 84-494.

TRW (TRW Environmental Safety Systems, Inc.), 1994, FY 93 thermal loading systems study final report:, B00000000-01717-5705-00013, Rev. 1, August 29, 1994, U.S. Department of Energy, Las Vegas, Nev.

Weeks, E.P., and Wilson, W.E., 1984, Preliminary evaluation of hydrologic properties of cores of unsaturated tuff, test well USW H-1, Yucca Mountain, Nevada: U.S. Geological Survey Water Resources Investigations Report 84-4193, U.S. Geological Survey, 30 p.

Wittwer, C.S., Bodvarsson, G.S., Chornack, M.P., Flint, A.L., Flint L.E., Lewis, B.D., and Rautman, C.A., 1992, Design of a three-dimensional site-scale model for the unsaturated zone at Yucca Mountain, Nevada, *in* High-Level Radioactive Waste Management, Proceedings of the Third International Conference, LaGrange Park, Ill.: American Nuclear Society, p. 263-271.

Yucca Mountain Project, 1992. Data resulting from data acquisition: Yucca Mountain Project Technical Data Information Form, DTN: GS920508312231.011.

This page intentionally left blank.

Color Figures
(Plates 1–7)

(This sheet and the color figures that follow are single sided.)

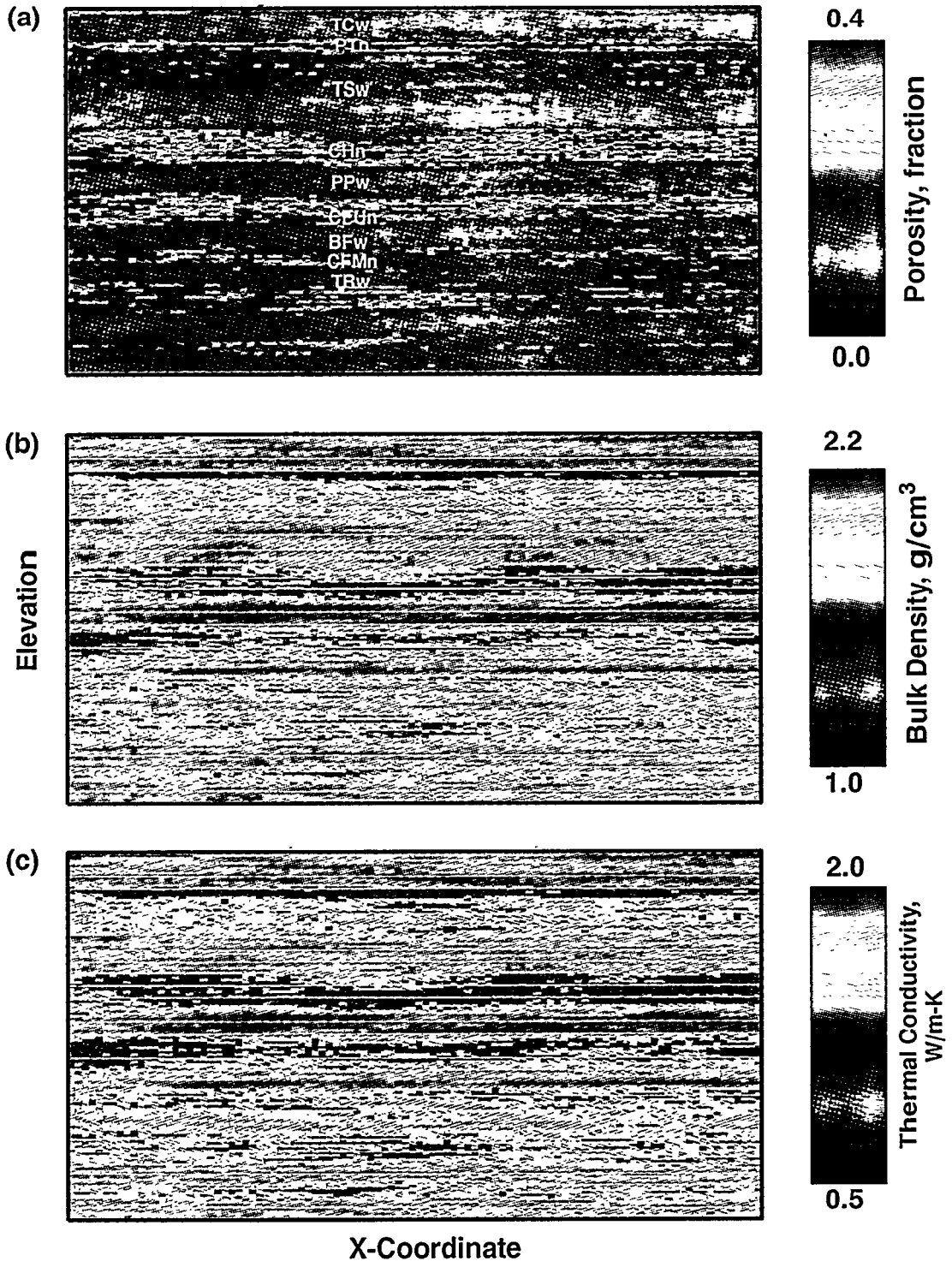

Plate 1. Color-coded images of material-properties models for (a) porosity, (b) bulk density, and (c) thermal conductivity corresponding to geostatistical model GC1HL of Longenbaugh and others (1995). Models are presented in stratigraphic coordinates (see text). Range of spatial correlation 5,000 m. Model dimensions and node spacings defined in figure 4.

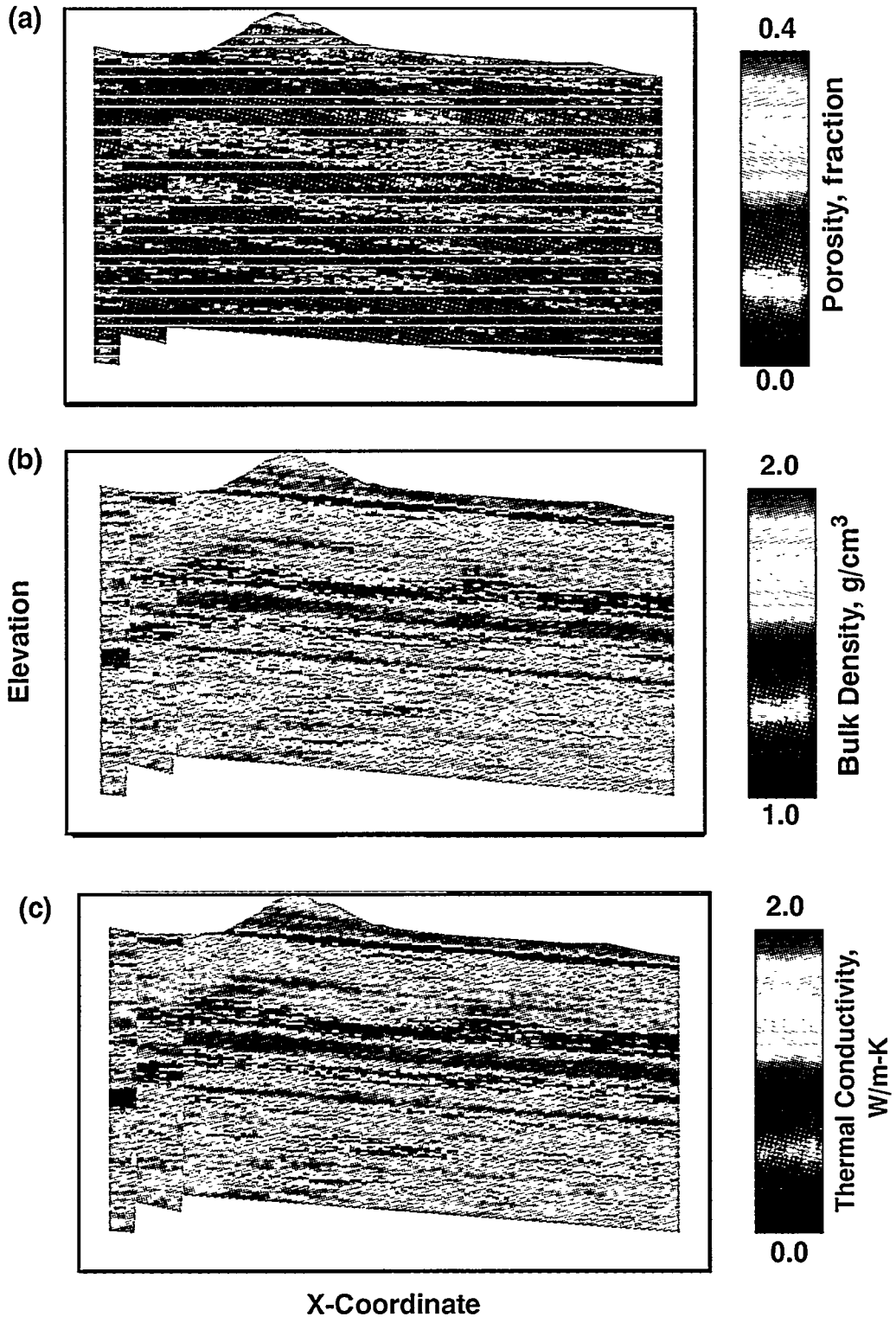

Plate 2. Color-coded images of post-processed material-properties models for (a) porosity, (b) bulk density, and (c) thermal conductivity corresponding to geostatistical model GC1HL of Longenbaugh and others (1995), showing tectonic dip and fault offsets. Compare with plate 1.

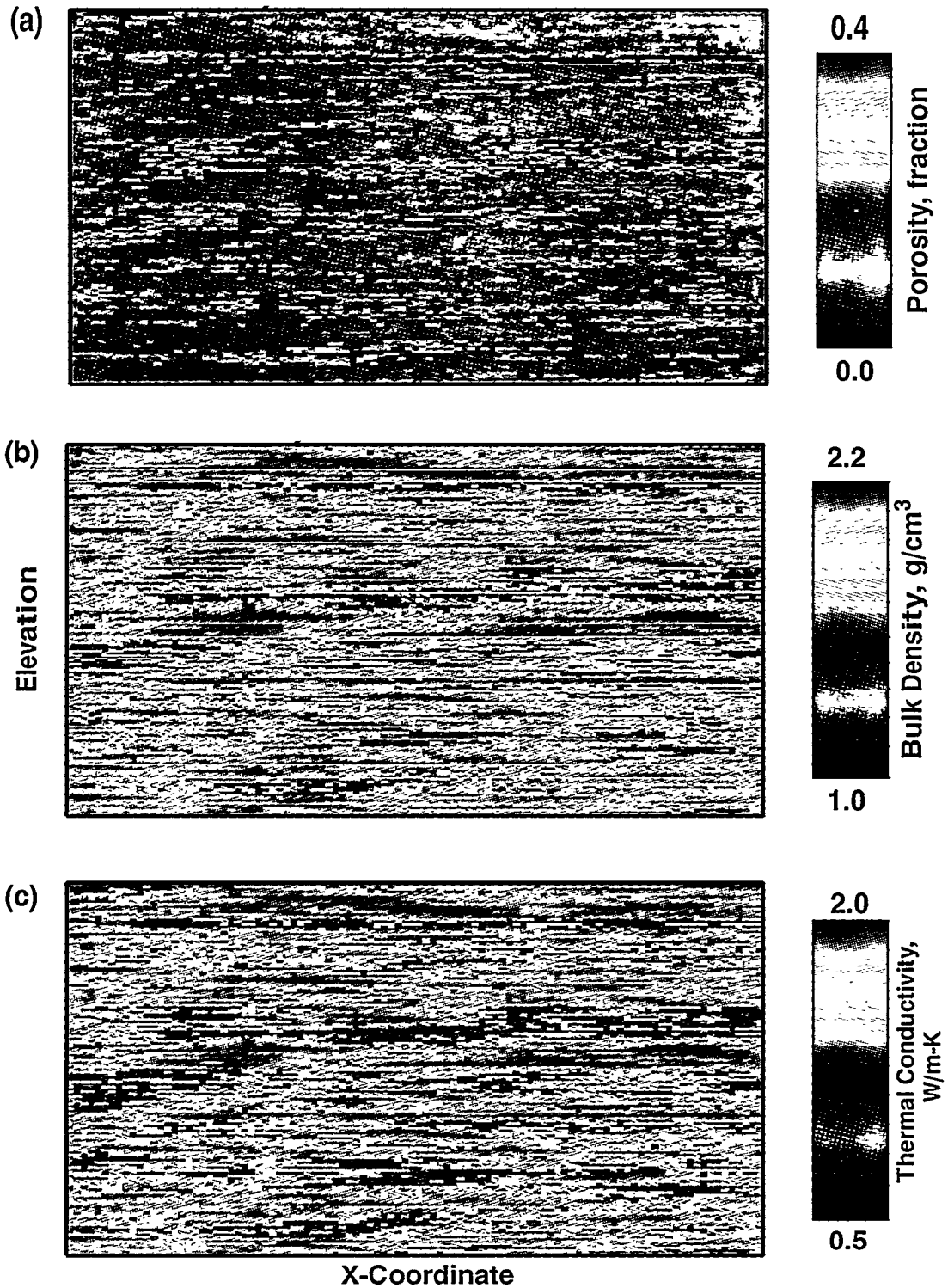

Plate 3. Color-coded images of material-properties models for (a) porosity, (b) bulk density, and (c) thermal conductivity corresponding to geostatistical model GC2HL. Models are presented in stratigraphic coordinates (see text). Range of spatial correlation 1,000 m. Model dimensions and node spacings defined in figure 4.

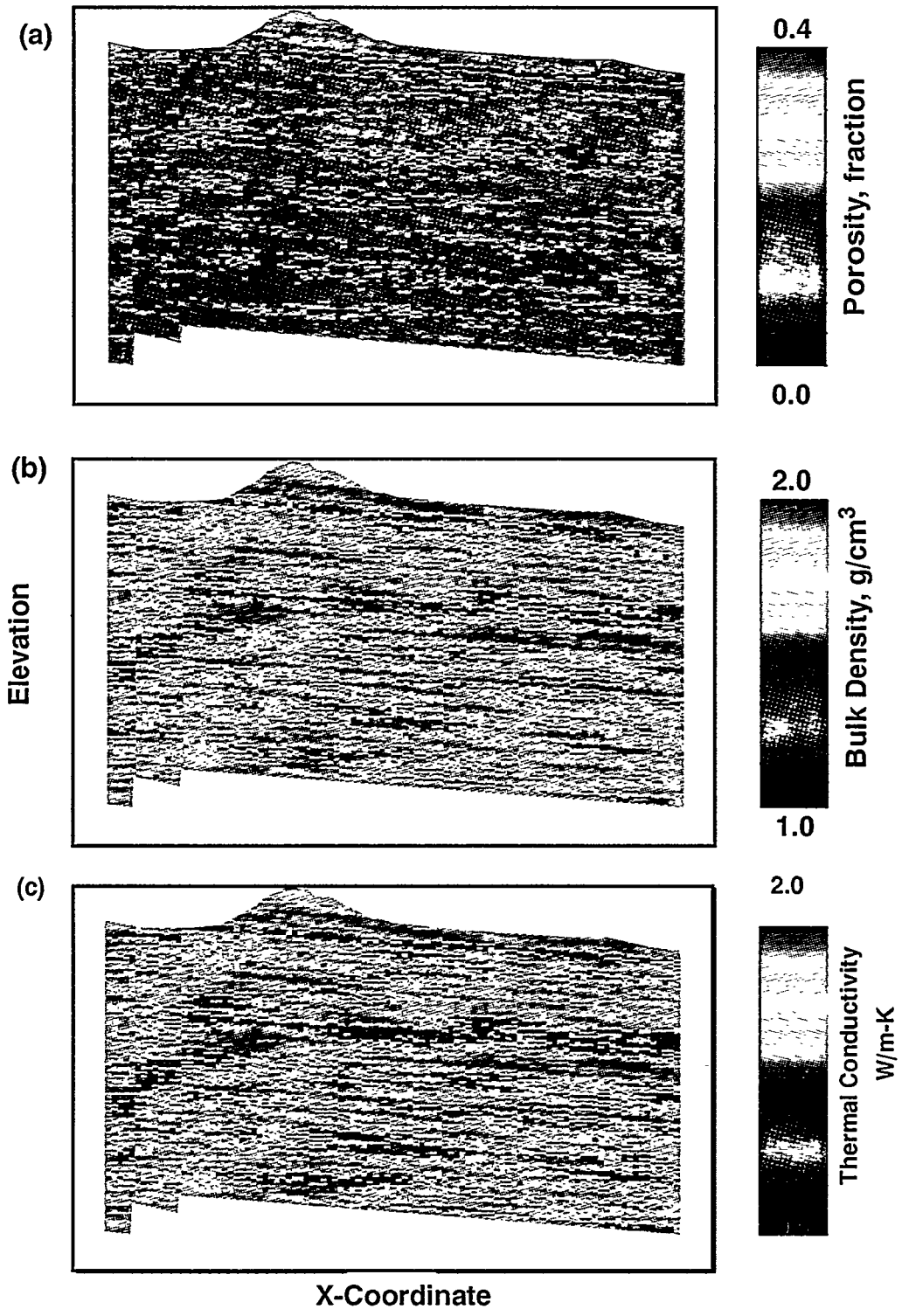

Plate 4. Color-coded images of post-processed material-properties models for (a) porosity, (b) bulk density, and (c) thermal conductivity corresponding to geostatistical model GC2HL, showing tectonic dip and fault offsets. Compare with plate 3.

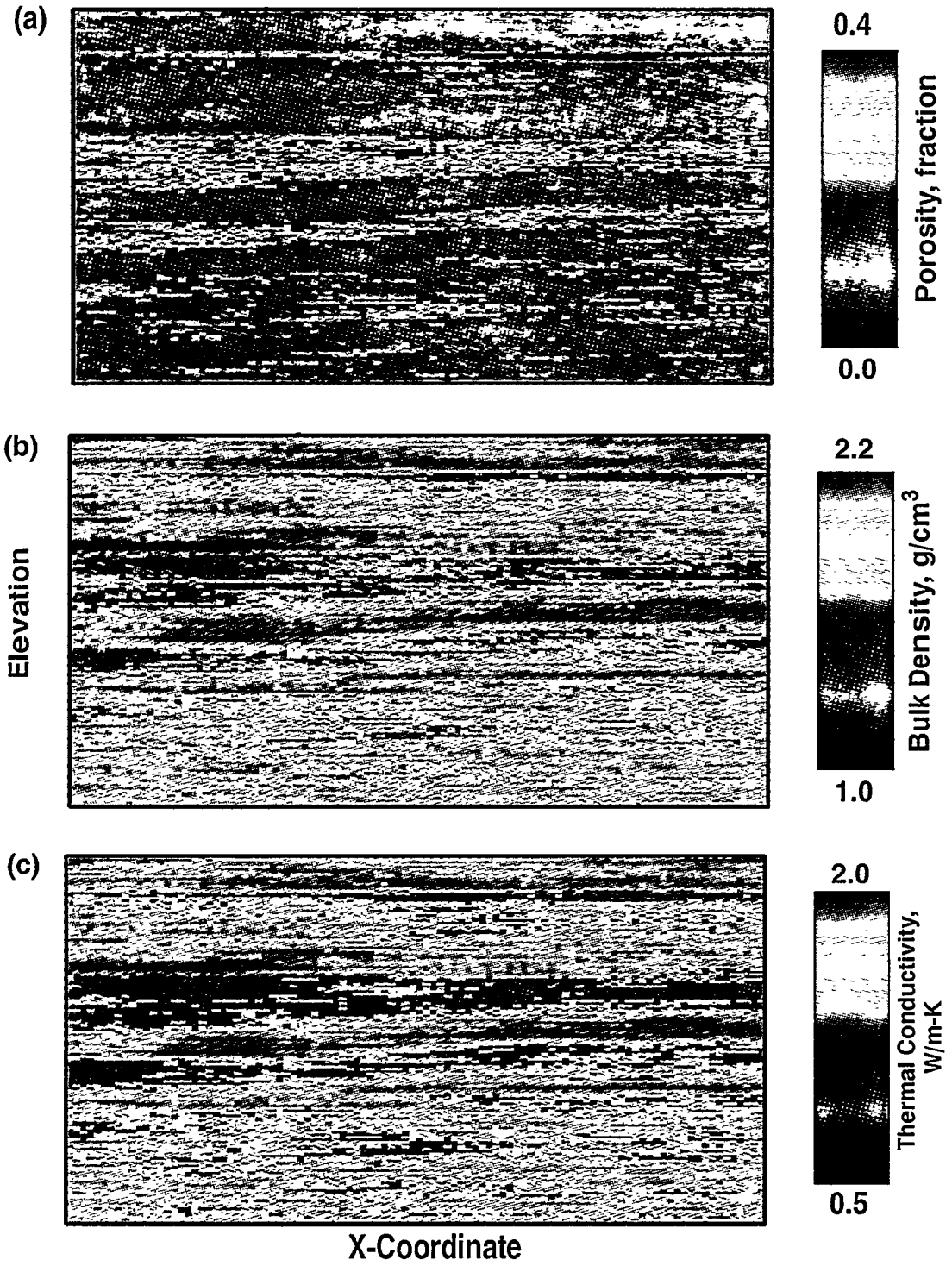

Plate 5. Color-coded images of material-properties models for (a) porosity, (b) bulk density, and (c) thermal conductivity corresponding to geostatistical model GC3HL. Models are presented in stratigraphic coordinates (see text). Range of spatial correlation 5,000 m. Conditioning data derived from drill holes USW GU-3/G-3, USW G-4, and UE-25 a#1. Model dimensions and node spacings defined in figure 4.

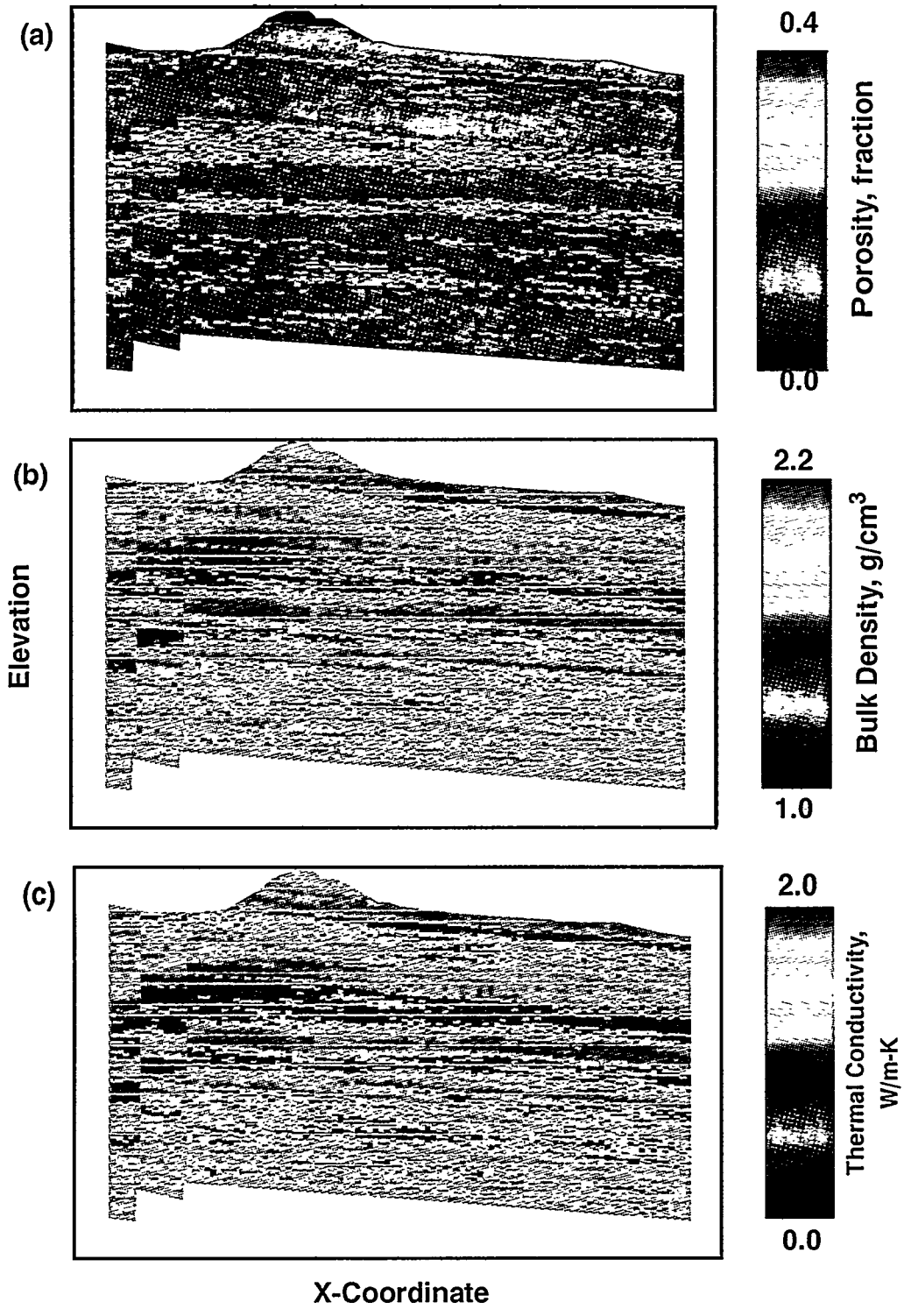

Plate 6. Color-coded images of post-processed material-properties models for (a) porosity, (b) bulk density, and (c) thermal conductivity corresponding to geostatistical model GC3HL, showing tectonic dip and fault offsets. Compare with plate 5.

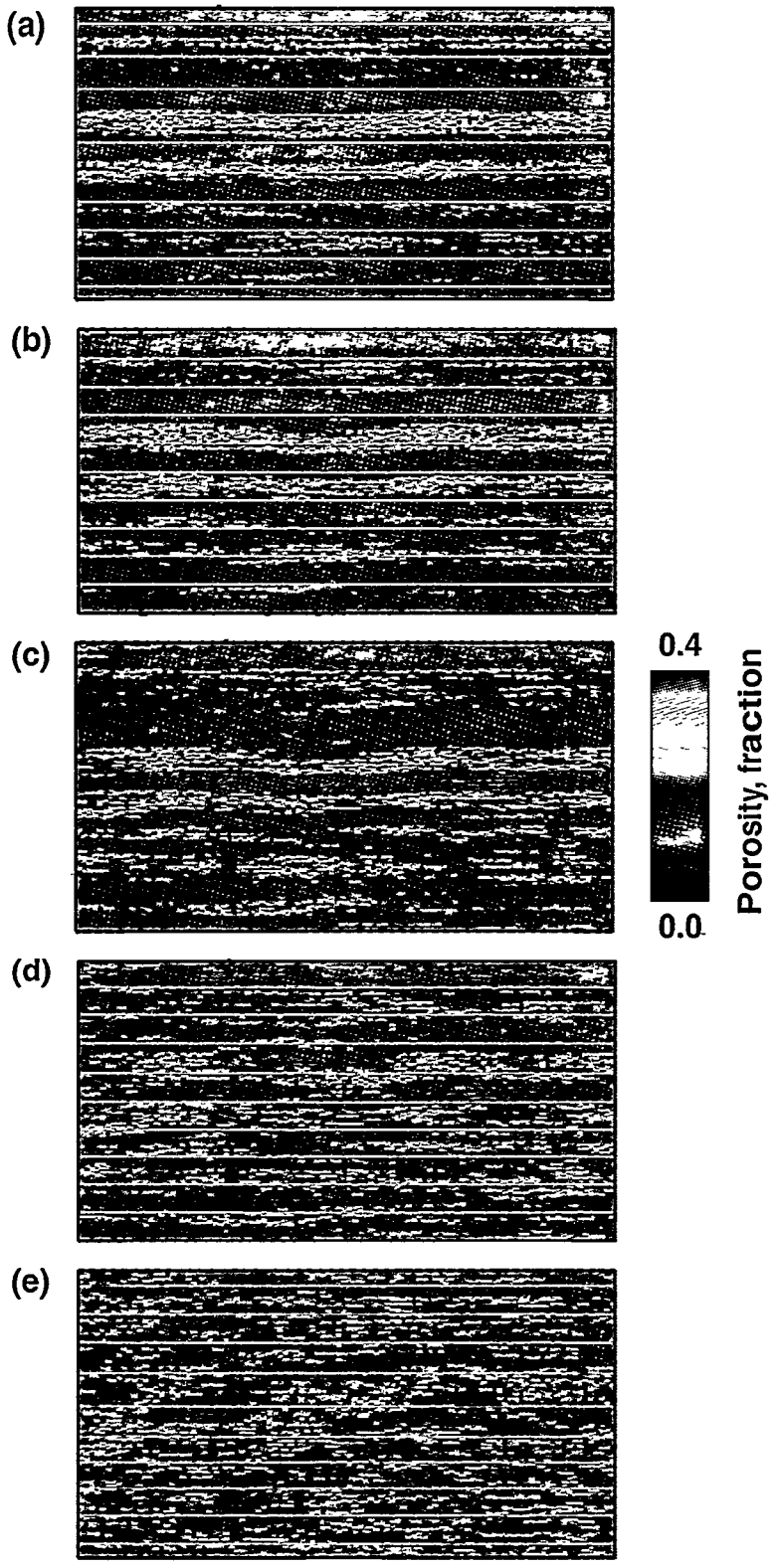

Plate 7. Comparison of the influence of spatial correlation length on models of porosity. (a) Range of correlation = 10,000 m; (b) 5,000 m (GC1HL); (c) 2,000 m; (d) 1,000 m (GC2HL); and (e) 500 m. Identical conditioning data used in each model.

Appendix

Additional Discussion of Porosity-Thermal Conductivity Relationship

The relationship between the thermal conductivity of tuff and porosity is critical to the modeling of heat dissipation by conduction using the latter property as a surrogate. Continuing concern regarding the porosity-thermal conductivity relationship presented in equation (2) has lead to additional evaluation of this relationship. These coefficients of the multiple regression equations (table 1) were provided based on incomplete laboratory testing information and general knowledge of the thermal behavior of tuffs. Different regression coefficients were used for welded and nonwelded materials. As stated in the body of this report, simple cross plots of thermal conductivity as a function of porosity indicated a strong relationship, despite the relatively low r^2 values or small sample size for some of the categories given in table 1. In the press of conducting both the geostatistical and thermal-process modeling to meet a Yucca Mountain Project milestone, this simple visual evaluation was judged sufficient confirmation of the provided relationships (C.S. Chocas, Sandia National Laboratories, written comm., 1994), and the stated coefficients were accepted. The purpose of the analyses, after all, was to evaluate the *effects* of spatial heterogeneity in contrast to other highly simplified assumptions regarding the distribution of material properties, notably thermal conductivity.

This appendix presents the results of an independent evaluation of the porosity-thermal conductivity relationship. For purposes of this evaluation, welded and nonwelded lithologic types have been aggregated to achieve a larger statistical mass (i.e., to avoid excessively small sample sizes). Although there are good theoretical reasons to expect different correlation relationships for welded and nonwelded tuffs, based principally on known differences in mineralogy between the two materials, the number of physical samples tested from Yucca Mountain at this time is insufficient to define these relationships with great confidence (e.g., table 1).

Figure A-1 presents a composite, simple linear regression computed for thermal conductivities, measured at various low temperatures (<100°C, i.e., below the boiling of contained pore water), as a function of porosity only. The effect of initial saturation has been ignored (the individual physical samples have been tested at varying saturations). This amounts to projecting measurements at different saturations onto the same porosity-thermal conductivity plane. The correlation shown in figure A-1 is quite good, even neglecting the influence of saturation. The coefficient of determination (r^2 value) is about 0.72, indicating that nearly 72 percent of the variation in measured thermal conductivity at three different sub-boiling temperatures is explained by variations in porosity, Note that the range of porosity values spans virtually the entire range expected at Yucca Mountain for both welded and nonwelded lithologies. The unequal variance of the residuals at various porosity levels is probably largely a function of differing numbers of measurements at those levels.

Figure A-2 is the comparable, composite linear regression for high temperature (>100°C) measurements. Again, there is a strong functional dependence at all initial temperatures on porosity. Variability in the measured values is reduced, in comparison with those shown in figure A-1, because all initial saturations at these above-boiling temperatures are equal to zero. The r^2 value for this simple linear regression is above 0.90. Thermal conductivities have been measured for samples spanning the entire range of welded and nonwelded rock types. Nonwelded samples (high porosity), however, are definitely under-represented at this stage of site characterization.

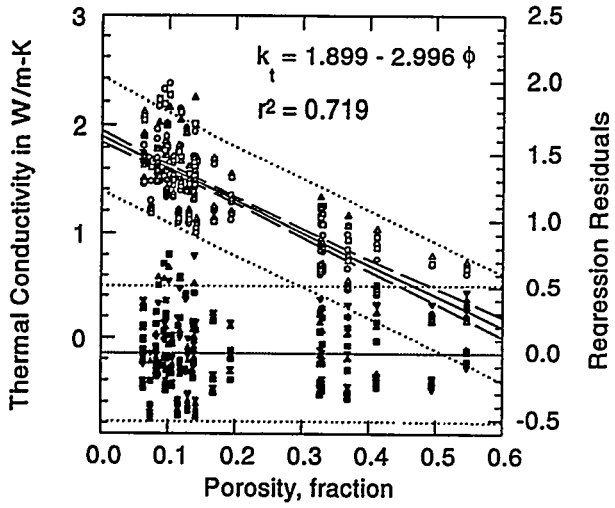

Figure A-1. Cross plot of measured thermal conductivity values at 30°, 50°, and 70°C (upper points) plotted as a function of porosity. Residuals from regression equation (solid line) shown on lower portion of diagram. Dashed and dotted lines are 95-percent confidence limits on regression equation and prediction interval, respectively.

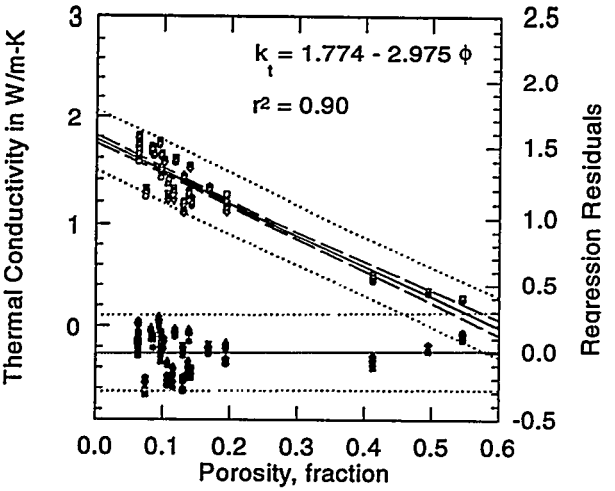

Figure A-2. Cross plot of measured thermal conductivity values at 110°, 155°, 200°, 245°, and 290°C (upper points) plotted as a function of porosity. Residuals from regression equation (solid line) shown on lower portion of diagram. Dashed and dotted lines are 95-percent confidence limits on regression equation and prediction interval, respectively.

The simple linear regression analyses of figures A-1 and A-2 confirm that modeling thermal conductivity using porosity as a surrogate material property is a reasonable approach. A non-quantitative, but instructive, evaluation of the specific coefficients from table 1 for the multiple-regression relationship (equation (2)) is presented in figure A-3. This perspective diagram presents the available thermal conductivity measurements (measured at 50°C) plotted as a function of both initial saturation and porosity. Also plotted on the figure is the surface representing the predicted thermal conductivity values at the same initial temperature across the full range of possible saturations and the range of observed porosity values (equation (2)). The effect of porosity clearly dominates both the measured and predicted thermal conductivity values.

This reevaluation of the porosity-thermal conductivity relationship indicates that the use of porosity as a surrogate material property is justified, and that the specific transformation used in the modeling described in the body of this report is a reasonable approximation of the true relationship at this state of site characterization. The specific coefficients should be updated in future, similar analyses as additional laboratory measurements are obtained.

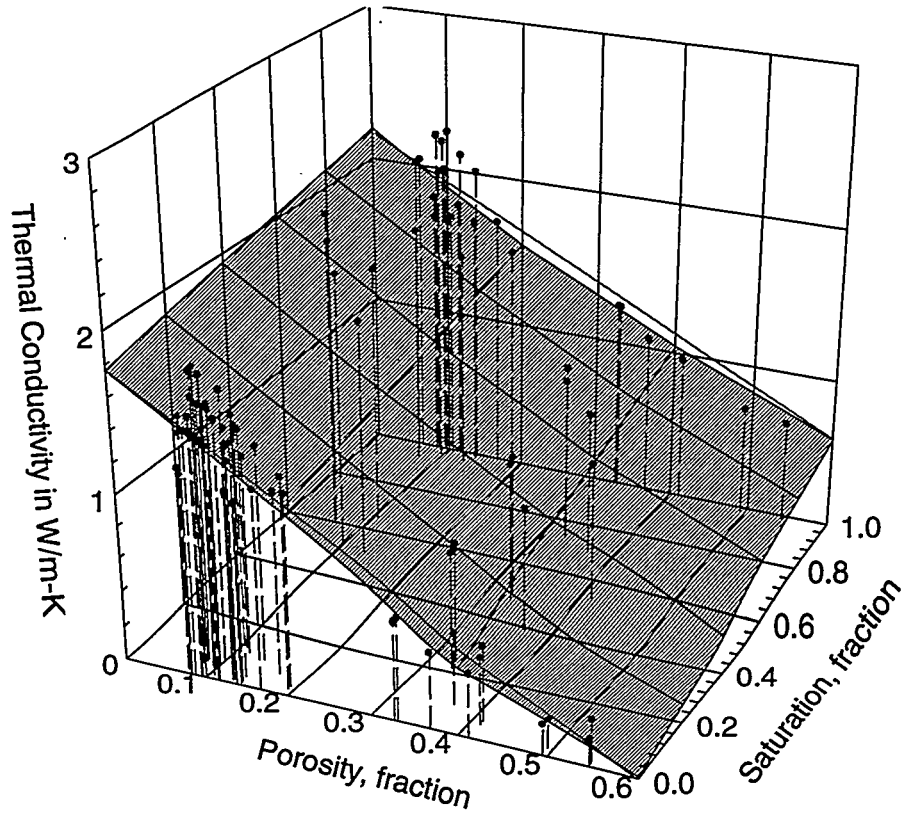

Figure A-3. Multivariate scatterplot of thermal conductivity values measured at 50 °C as a function of porosity and initial saturation. Measurements are projected (dashed lines) onto the porosity-saturation plane for better visualization. Shaded surface represents multiple linear regression prediction from equation (2) using coefficients from table 1. Straight bounding lines (front and back) added to emphasize non-planar nature of surface.

YUCCA MOUNTAIN SITE CHARACTERIZATION PROJECT

UC814 - DISTRIBUTION LIST

1 D. A. Dreyfus (RW-1)
Director
OCRWM
US Department of Energy
1000 Independence Avenue SW
Washington, DC 20585

1 L. H. Barrett (RW-2)
Acting Deputy Director
OCRWM
US Department of Energy
1000 Independence Avenue SW
Washington, DC 20585

1 S. Rousso (RW-40)
Office of Storage and Transportation
OCRWM
US Department of Energy
1000 Independence Avenue SW
Washington, DC 20585

1 R. A. Milner (RW-30)
Office of Program Management
and Integration
OCRWM
US Department of Energy
1000 Independence Avenue SW
Washington, DC 20585

1 D. R. Elle, Director
Environmental Protection Division
DOE Nevada Field Office
US Department of Energy
P.O. Box 98518
Las Vegas, NV 89193-8518

1 T. Wood (RW-14)
Contract Management Division
OCRWM
US Department of Energy
1000 Independence Avenue SW
Washington, DC 20585

4 Victoria F. Reich, Librarian
Nuclear Waste Technical Review Board
1100 Wilson Blvd., Suite 910
Arlington, VA 22209

5 Wesley Barnes, Project Manager
Yucca Mountain Site Characterization
Office
US Department of Energy
P.O. Box 98608--MS 523
Las Vegas, NV 89193-8608

1 Director
Office of Public Affairs
DOE Nevada Operations Office
US Department of Energy
P.O. Box 98518
Las Vegas, NV 89193-8518

8 Technical Information Officer
DOE Nevada Operations Office
US Department of Energy
P.O. Box 98518
Las Vegas, NV 89193-8518

1 P. K. Fitzsimmons, Technical Advisor
Office of Assistant Manager for
Environmental Safety and Health
DOE Nevada Operations Office
US Department of Energy
P.O. Box 98518
Las Vegas, NV 89193-8518

1 J. A. Blink
Deputy Project Leader
Lawrence Livermore National Laboratory
101 Convention Center Drive
Suite 820, MS 527
Las Vegas, NV 89109

2 J. A. Canepa
Technical Project Officer - YMP
N-5, Mail Stop J521
Los Alamos National Laboratory
P.O. Box 1663
Los Alamos, NM 87545

1 Repository Licensing & Quality
Assurance
Project Directorate
Division of Waste Management
US NRC
Washington, DC 20555

1 Senior Project Manager for Yucca
Mountain
Repository Project Branch
Division of Waste Management
US NRC
Washington, DC 20555

1 NRC Document Control Desk
Division of Waste Management
US NRC
Washington, DC 20555

1 Chad Glenn
NRC Site Representative
301 E Stewart Avenue, Room 203
Las Vegas, NV 89101

1 E. P. Binnall
Field Systems Group Leader
Building 50B/4235
Lawrence Berkeley Laboratory
Berkeley, CA 94720

1 Center for Nuclear Waste
Regulatory Analyses
6220 Culebra Road
Drawer 28510
San Antonio, TX 78284

2 W. L. Clarke
Technical Project Officer - YMP
Attn: YMP/LRC
Lawrence Livermore National Laboratory
P.O. Box 5514
Livermore, CA 94551

1 V. R. Schneider
Asst. Chief Hydrologist -- MS 414
Office of Program Coordination
and Technical Support
US Geological Survey
12201 Sunrise Valley Drive
Reston, VA 22092

1 J. S. Stuckless, Chief
Geologic Studies Program
MS 425
Yucca Mountain Project Branch
US Geological Survey
P.O. Box 25046
Denver, CO 80225

1 N. Z. Elkins
Deputy Technical Project Officer
Los Alamos National Laboratory
Mail Stop 527
101 Convention Center Drive, #820
Las Vegas, NV 89109

2 Michaele C. Brady
Technical Project Officer - YMP
Sandia National Laboratories
Organization 6302, MS 1399
101 Convention Center Drive, Suite 880
Las Vegas, NV 89109

1 Ray Wallace
US Geological Survey
106 National Center
12201 Sunrise Valley Drive
Reston, VA 22092

1 L. R. Hayes
Technical Project Officer
Yucca Mountain Project Branch
MS 425
US Geological Survey
P.O. Box 25046
Denver, CO 80225

2 A. L. Flint
US Geological Survey
MS 721
P.O. Box 327
Mercury, NV 89023

1 R. E. Lewis
Yucca Mountain Project Branch
MS 425
US Geological Survey
P.O. Box 25046
Denver, CO 80225

1 D. Zesiger
US Geological Survey
101 Convention Center Drive
Suite 860, MS 509
Las Vegas, NV 89109

2 L. D. Foust
Nevada Site Manager
TRW Environmental Safety Systems
101 Convention Center Drive
Suite P-110, MS 423
Las Vegas, NV 89109

1 C. E. Ezra
YMP Support Office Manager
EG&G Energy Measurements Inc.
MS V-02
P.O. Box 1912
Las Vegas, NV 89125

1 E. L. Snow, Program Manager
Roy F. Weston, Inc.
955 L'Enfant Plaza SW
Washington, DC 20024

1 Technical Information Center
Roy F. Weston, Inc.
955 L'Enfant Plaza SW
Washington, DC 20024

1 Technical Project Officer - YMP
US Bureau of Reclamation
Code D-3790
P.O. Box 25007
Denver, CO 80225

1 B. T. Brady
Records Specialist
US Geological Survey
MS 421
P.O. Box 25046
Denver, CO 80225

1 M. D. Voegele
Technical Project Officer - YMP
M&O/SAIC
101 Convention Center Drive
Suite 407
Las Vegas, NV 89109

1 Paul Eslinger, Manager
PASS Program
Pacific Northwest Laboratories
P.O. Box 999
Richland, WA 99352

1 A. T. Tamura
Science and Technology Division
OSTI
US Department of Energy
P.O. Box 62
Oak Ridge, TN 37831

1 P. J. Weeden, Acting Director
Nuclear Radiation Assessment Div.
US EPA
Environmental Monitoring Sys. Lab
P.O. Box 93478
Las Vegas, NV 89193-3478

1 ONWI Library
Battelle Columbus Laboratory
Office of Nuclear Waste Isolation
505 King Avenue
Columbus, OH 43201

1 C. H. Johnson
Technical Program Manager
Agency for Nuclear Projects
State of Nevada
Evergreen Center, Suite 252
1802 N. Carson Street
Carson City, NV 89710

1 John Fordham, Deputy Director
Water Resources Center
Desert Research Institute
P.O. Box 60220
Reno, NV 89506

1 The Honorable Cyril Schank
Chairman
Churchill County Board of
Commissioners
190 W. First Street
Fallon, NV 89406

1 T. Hay, Executive Assistant
Office of the Governor
State of Nevada
Capitol Complex
Carson City, NV 89710

3 R. R. Loux
Executive Director
Agency for Nuclear Projects
State of Nevada
Evergreen Center, Suite 252
1802 N. Carson Street
Carson City, NV 89710

1 Brad R. Mettam
Inyo County Yucca Mountain
Repository Assessment Office
P. O. Drawer L
Independence, CA 93526

1 Lander County Board of Commissioners
315 South Humbolt Street
Battle Mountain, NV 89820

1 Vernon E. Poe
Office of Nuclear Projects
Mineral County
P.O. Box 1600
Hawthorne, NV 89415

1 Les W. Bradshaw
Program Manager
Nye County Nuclear Waste Repository
Project Office
P.O. Box 1767
Tonopah, NV 89049

1 Florindo Mariani
White Pine County Coordinator
P. O. Box 135
Ely, NV 89301

1 Judy Foremaster
City of Caliente Nuclear Waste
Project Office
P.O. Box 158
Caliente, NV 89008

1 Philip A. Niedzielski-Eichner
Nye County Nuclear Waste
Repository Project Office
P.O. Box 221274
Chantilly, VA 22022-1274

1 Dennis Bechtel, Coordinator
Nuclear Waste Division
Clark County Department of
Comprehensive Planning
301 E. Clark Avenue, Suite 570
Las Vegas, NV 89101

1 Juanita D. Hoffman
Nuclear Waste Repository
Oversight Program
Esmeralda County
P.O. Box 490
Goldfield, NV 89013

1 Eureka County Board of Commissioners
Yucca Mountain Information Office
P.O. Box 714
Eureka, NV 89316

1 Economic Development Dept.
City of Las Vegas
400 E. Stewart Avenue
Las Vegas, NV 89101

1 Community Planning & Development
City of North Las Vegas
P.O. Box 4086
North Las Vegas, NV 89030

1 Community Development & Planning
City of Boulder City
P.O. Box 61350
Boulder City, NV 89006

1 Commission of European Communities
200 Rue de la Loi
B-1049 Brussels
BELGIUM

2 Librarian
YMP Research & Study Center
MS 407
P.O. Box 98521
Las Vegas, NV 89193-8521

1 Amy Anderson
Argonne National Laboratory
Building 362
9700 S. Cass Avenue
Argonne, IL 60439

1 Glenn Van Roekel
Director of Community Development
City of Caliente
P.O. Box 158
Caliente, NV 89008

3 G. S. Bodvarsson
Head, Nuclear Waste Department
Lawrence Berkeley Laboratory
1 Cyclotron Road, MS 50E
Berkeley, CA 94720

1 Michael L. Baughman
Intertech Services Corp.
P.O. Box 93537
Las Vegas, NV 89193

3 Yucca Mountain Site Characterization
Project Office
U. S. Department of Energy
Attn: J. C. DeLaGarza
P200-217
P. O. Box 98608
Las Vegas, NV 89193-8608

3 M&O/TRW
Attn: S. F. Saterlie
9200-J
101 Convention Center Drive
Las Vegas, NV 89109

1 M&O/WCFS
J. R. Gauthier
MS 1326

2 Yucca Mountain Site Characterization
Project Office
U. S. Department of Energy
Attn: M. C. Tynan
P200-217
P. O. Box 98608
Las Vegas, NV 89193-8608

	MS	
2	1330	C. B. Michaels, 6352 100/1.2.3.2.2.2.2 /SAND94-2283/QA
20	1330	WMT Library, 6352
2	1325	E. E. Ryder
1	0974	R. S. Longsbaugh
1	1325	L. S. Costin
1	1324	C. S. Chocas
1	1326	N. D. Francis
10	1324	C. Rautman
1	9018	Central Technical Files, 8523-2
5	0899	Technical Library, 13414
1	0619	Print Media, 12615
2	0100	Document Processing, 7613-2 for DOE/OSTI